A wavelet method for reducing the computational cost of BE-based homogenization analysis

Kazuhiro Koro*, Kazuhisa Abe†

Department of Civil Engineering and Architecture, Niigata University
8050 Igarashi 2-Nocho, Niigata, 950-2181, JAPAN

*Associate Professor, E-mail; kouro@eng.niigata-u.ac.jp
†Corresponding Author, Associate Professor, Fax; +81-25-262-7021, E-mail; abe@eng.niigata-u.ac.jp

Summary

A wavelet BEM is applied to the evaluation of the effective elastic moduli of unidirectional composites, based on the homogenization theory. This attempt is devoted to the reduction of computational cost for the BE-based homogenization analysis. Truncation for matrix compression is carried out by the Beylkin-type algorithm. A thresholding value for the truncation is set such that the discretization error of BE solution is comparable to its truncation error. Besides, rearrangement of the BE equations is proposed to attain rapid convergence of iterative solutions. Through investigation of asymptotical convergence of the effective moduli, it is found that the BE-based homogenization analysis ensures the same rate of convergence for effective moduli as for characteristic functions. By applying the wavelet BEM to heterogeneous media which have microstructures with many voids, the effective moduli with agreement of $2 - 4$ digits can be evaluated using $20 - 50$ % memory requirements of conventional BE approaches.

Key Words

Homogenization method, Wavelet BEM, Haar wavelets, Effective elastic modulus, Unidirectional composites

1 Introduction

The homogenization method is one of the mechanical and mathematical tools for evaluating macroscopic effective property of microscopic heterogeneous media. In formulation of the homogenization method, it is supposed that a microstructure defining a state of heterogeneity possesses spatial periodicity in a body. Then, the phase of the microstructure is represented by so-called *a unit cell* or *a representative volume element (RVE)*. In this stage, we consider an infinitesimal size of the unit cell, and hence we can model the microscopic heterogeneous problems as a coupling of two boundary value problems concerning microscopic- and macroscopic fields. As a result, the macroscopic responses in the *homogenized* field can be described based on the constitutive law defined by the ensemble averages of microscopic variables. On the other hand, a state of microscopic field, e.g. stress distribution in a unit cell embedded in the homogenized field, can be easily simulated based on macroscopic responses.

The homogenization approach has several outstanding advantages. One is that the consistency in mathematical and physical aspects inheres in the multi-scale modeling, which is not seen in the classical micromechanics (e.g. [1]) and the conventional numerical RVE analysis (e.g. [2]). In the formulation, two variables are introduced to describe the states of the fields. These are independent of each other in the macroscopic- and microscopic fields; nevertheless, both variables strictly satisfy the governing equation in each field. Another advantage is the availability of widely-used numerical tools in both macroscopic- and microscopic analyses. Besides, there are no restrictions on the phases of microstructures. We can therefore, analyze the effective properties and the macroscopic responses of a wide class of heterogeneous media. The engineering use of the homogenization method has been introduced in vast papers (e.g. [3][4][5]); most of these numerical results have been obtained by finite element (FE) analysis. This is due to wide applicability of the FEM.

The homogenization analysis however, has the mesh sensitivity on evaluation of the effective moduli. This has been pointed out by Guedes & Kikuchi [3]. To overcome this difficulty, they [3] have attempted to apply a mesh adaptation algorithm to the homogenization analysis. Their attempt attains remarkable improvement in the asymptotical rate of effective moduli. If we do not use such algorithms to retain the accuracy of the effective moduli, we will certainly need a large number of finite elements. In implementation of FE-based analysis, the increase in the number of finite elements will incur the difficulty of mesh generation.

These computational problems in the FE-based homogenization analysis can be settled by application of the BEM, because the procedure for evaluating effective moduli based on the FEM can be quite replaced to the BE-based procedure. In the BE-based homogenization analysis, the effective moduli can be evaluated by calculation of the boundary integrals concerning characteristic functions [6]. Hence, it is expected that the asymptotical convergence rates of the effective moduli are the same as those of the characteristic functions. Besides, only meshing on boundary is required in implementation of BE-based

analysis, which also alleviates the difficulty of mesh generation. Therefore, several researchers have attempted to apply the BEM to homogenization analysis, e.g. Kamiński [7], Okada et al. [6] and Procházka [8][9].

Although the BE-based homogenization analysis leads to the reduction of the task for pre-processing, a computational problem peculiar to BE analysis — large computational cost in large-scale problems — still remains in its implementation. This difficulty in particular will be serious for such microscopic problems as the microstructure with many particles, many fissures or cracks, and with stress concentration, for which we have to treat the boundary element equations with large degree of freedom in order to evaluate the effective moduli with sufficient accuracy. In such a situation, application of a wavelet BEM may be effective for the reduction of computational cost for the BE-based homogenization analysis.

The wavelet BEM has a simple algorithm in which wavelet bases are employed as basis functions for the discretization of boundary integral equation (BIE) [10]. In this method, the far-field influences in the BIE decay more rapidly due to vanishing moments of wavelets than that in the conventional BE analysis [11]. By applying the wavelet algorithm to the BEM, we consequently obtain a coefficient matrix of which most of entries have small values owing to the rapid decay. This matrix however, remains a fully populated one in this stage. It turns to a sparse coefficient matrix by truncation of these small matrix entries. A sparse matrix enables us to reduce not only the memory requirements, but also the CPU time for BE analysis with application of iterative solvers. In BE analysis, the wavelet method may enhance the computational performance up to $O(N(\log N)^{\alpha})$ $(\alpha \geq 0)$ or $O(N^{1+\gamma})$ $(0 \leq \gamma < 1)$ storage memory and complexity. Its availability to saving of computational cost has been verified through numerical results in many papers, e.g. [12][13][14][15][16][17][18].

In this paper, the fundamental aspects in the implementation of the wavelet BEM for homogenization analysis and its availability are discussed. The outline of this paper is as follows. In Section 2, we describe the boundary integral formulation for evaluating the effective elastic moduli of unidirectional composites. As will be mentioned in the present paper, this formulation is based on the mathematical homogenization theory introduced in Ref. [3]. In Section 3, we introduce several numerical procedures required to implement the wavelet BEM in the homogenization analysis. The discussion presented in this section is comprised of the following aspects; discretization, treatment of periodic boundary conditions, equation rearrangement that yields rapid convergence of the iterative solution, and matrix compression strategy. In Section 4, we first describe an algorithm of the wavelet BEM used in the homogenization analysis for unidirectional composites. The remainder of this section is devoted to presentation of basic performance of homogenization analysis based on the wavelet BEM. We investigate, in particular, the availability of the several manipulations introduced in implementation of wavelet BEM and the behavior of errors of the effective elastic moduli evaluated using the wavelet BEM. Finally, concluding remarks are summarized in Section 5.

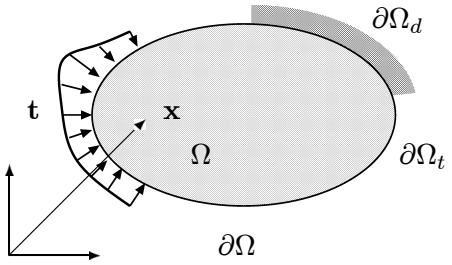

Figure 1: A state of equilibrium of a heterogeneous elastic body.

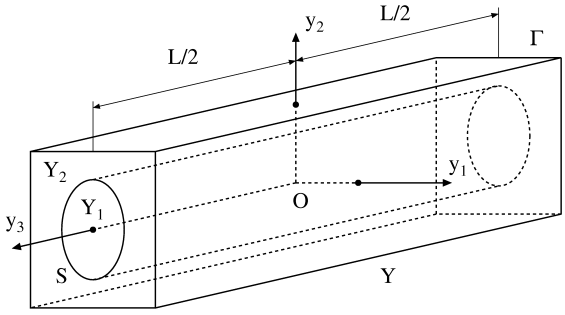

Figure 2: Microstructure of unidirectional composites.

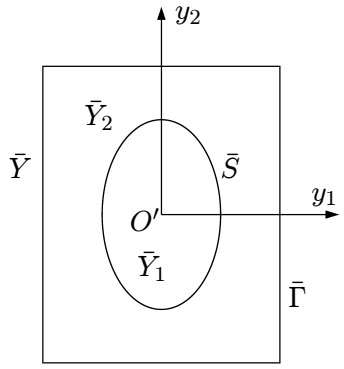

Figure 3: Phase of constituents in $y_1 - y_2$ plane.

2 Boundary integral formulation for evaluating effective elastic moduli of unidirectional composites

Let us consider the effective elastic modulus of a heterogeneous medium illustrated in Figure 1. We suppose that the medium is the two-phase material comprised of inclusion- and matrix phases. All the inclusions have a cylindrical shape, and are oriented toward a certain direction. Moreover, the representative length ε, by which the phases of the inclusions are specified, is very small in comparison with the scale of the overall elastic body shown in Figure 1.

To evaluate the effective elastic modulus of such a heterogeneous body, we now introduce the homogenization theory. In the mathematical homogenization, we suppose the spatial periodic arrangement of the cylindrical inclusions. Hence, the phase of the unidirectional composite can be specified by a unit cell illustrated in Figure 2. In the unit cell Y, the inclusion Y_1 and the matrix Y_2 are assumed to be perfectly bonded at the interface S.

As will be described in the below, the heterogeneous medium is regarded as a homogeneous elastic body under macroscopic coordinates $\mathbf{x}$, by using the homogenization theory. This macroscopic homogenized medium is subjected to the prescribed traction $\mathbf{t}$ on the

subboundary $\partial\Omega_t$ (see Figure 1). Note that we now neglect the body forces subjecting in the domain Ω for brevity. In this situation, a state of equilibrium of the medium can be described by a weak-form as follows:

$$\begin{aligned} &\int_{\Omega^\varepsilon} E^\varepsilon_{ijkl}\frac{\partial u^\varepsilon_k}{\partial x_l}\frac{\partial v_i}{\partial x_j}\,d\Omega = \int_{\partial\Omega_t} t_i v_i\,d(\partial\Omega), \\ &(\mathbf{u}^\varepsilon \in V^\varepsilon,\ \mathbf{v}\in V^\varepsilon), \qquad V^\varepsilon := \left\{\mathbf{v}\in (H^1(\Omega^\varepsilon))^3 |\quad \mathbf{v}=\mathbf{0}\ (\text{on}\ \partial\Omega_d)\right\}, \end{aligned} \tag{1}$$

where $\mathbf{u}^\varepsilon$ is the displacement in the domain Ω^ε of the heterogeneous medium with the periodic microstructure. The boundary $\partial\Omega$ consists of $\partial\Omega = \partial\Omega_d + \partial\Omega_t$. $\partial\Omega_d$ denotes the subboundary on which $\mathbf{u}^\varepsilon$ is prescribed. Moreover, the constitutive law of the heterogeneous medium is defined by

$$\sigma^\varepsilon_{ij} = E^\varepsilon_{ijkl}e^\varepsilon_{kl}, \qquad e^\varepsilon_{kl} = \frac{1}{2}\left(\frac{\partial u^\varepsilon_k}{\partial x_l} + \frac{\partial u^\varepsilon_l}{\partial x_k}\right), \tag{2}$$

$$E^\varepsilon_{ijkl} = \Theta_\alpha E^{(\alpha)}_{ijkl}, \quad (\alpha = 1,2), \qquad \Theta_\alpha = \begin{cases} 1, & \mathbf{y}\in Y_\alpha, \\ 0, & \text{elsewhere}, \end{cases} \tag{3}$$

$$E^\varepsilon_{ijkl} = E^\varepsilon_{jikl} = E^\varepsilon_{ijlk} = E^\varepsilon_{klij}, \quad C>0: \quad E^\varepsilon_{ijkl}e^\varepsilon_{ij}e^\varepsilon_{kl} \geq Ce^\varepsilon_{ij}e^\varepsilon_{ij}, \quad e^\varepsilon_{ij} = e^\varepsilon_{ji}, \tag{4}$$

where $\mathbf{y} = \mathbf{x}/\varepsilon$ is the coordinates for describing a state of the heterogeneous microscopic field. σ^ε_{ij} and e^ε_{ij} are the stress- and the strain tensors in Ω^ε, respectively. E^ε_{ijkl} is the elastic modulus of the medium, and $E^{(\alpha)}_{ijkl}$ represents the elastic modulus of the constituent Y_α.

In equation (1), the displacement $\mathbf{u}^\varepsilon$ varies within a small unit cell, and hence this variable depends not only on the macroscopic coordinates $\mathbf{x}$ but also on the microscopic coordinates $\mathbf{y}$. Furthermore, we assume that $\mathbf{u}^\varepsilon$ can be expressed by the following asymptotical expansion with respect to ε:

$$\mathbf{u}^\varepsilon = \mathbf{u}(\mathbf{x},\mathbf{y}) = \mathbf{u}^0(\mathbf{x},\mathbf{y}) + \varepsilon\mathbf{u}^1(\mathbf{x},\mathbf{y}) + \varepsilon^2(\cdots\cdots), \qquad \mathbf{y} = \frac{\mathbf{x}}{\varepsilon}, \tag{5}$$

where $\mathbf{u}^j(\mathbf{x},\mathbf{y})$ $(j=0,1,\ldots)$ is defined in $(\mathbf{x},\mathbf{y})\in\Omega\times Y$, and is periodic on $\mathbf{y}$ due to the periodicity of microstructure.

Substituting equation (5) into equation (1) and taking the limit $\varepsilon\longrightarrow 0^+$, we obtain the equilibrium equation of the macroscopic homogenized elastic body as follows [3]:

$$\begin{aligned} &\int_\Omega D_{ijkl}\frac{\partial u^0_k}{\partial x_l}(\mathbf{x})\frac{\partial v_i}{\partial x_j}(\mathbf{x})\,d\Omega = \int_{\partial\Omega_t} t_i v_i(\mathbf{x})\,d(\partial\Omega), \\ &\mathbf{v}\in V_\Omega, \quad V_\Omega := \{\mathbf{v}(\mathbf{x}) \text{ defined in } \Omega\,|\mathbf{v}=\mathbf{0}\ (\text{on}\ \partial\Omega_d);\ \mathbf{v} \text{ smooth enough}\}, \end{aligned} \tag{6}$$

$$D_{ijkl}(\mathbf{x}) := \frac{1}{|Y|}\int_Y \Theta_\alpha\left(E^{(\alpha)}_{ijkl} - E^{(\alpha)}_{ijpm}\frac{\partial\chi^{kl}_p}{\partial y_m}\right)dY, \tag{7}$$

$$D_{ijkl} = D_{jikl} = D_{ijlk} = D_{klij}, \quad C>0:\ D_{ijkl}e_{ij}e_{kl} \geq Ce_{ij}e_{ij}, \quad e_{ij} = e_{ji},$$

where the microscopic displacement $\mathbf{u}^0$ is independent of the variable $\mathbf{y}$, and D_{ijkl} is the effective elastic modulus of the homogenized medium. Furthermore, the function $\boldsymbol{\chi}^{kl}$,

which is essential to evaluate the effective modulus D_{ijkl}, is referred to as *the characteristic function*. This function is defined as a solution of the following microscopic boundary value problem:

$$\int_Y \Theta_\alpha E^{(\alpha)}_{ijpm} \frac{\partial \chi^{kl}_p}{\partial y_m} \frac{\partial v_i}{\partial y_j} dY = \int_Y \Theta_\alpha E^{(\alpha)}_{ijkl} \frac{\partial v_i}{\partial y_j} dY, \qquad \mathbf{v} \in V_Y,\ \boldsymbol{\chi}^{kl} \in V_Y, \tag{8}$$
$$V_Y := \{\mathbf{v}(\mathbf{y}) \text{ defined in } Y \,|\mathbf{v}(\mathbf{y}) \text{ Y} - \text{periodic};\ \mathbf{v} \text{ smooth enough}\}.$$

where "Y-periodic" implies the spatial periodicity of the microstructure. Notice that equation (8) implies that the characteristic function $\boldsymbol{\chi}^{kl}$ satisfies the equilibrium equation of elastic media [3][7]. Because of $\boldsymbol{\chi}^{kl} = \boldsymbol{\chi}^{lk}$, we need to solve equation (8) 3 times for 2-D or 6 times for 3-D, in the analysis. If the phase of the microstructure is specified by a unit cell, the procedure for evaluating the effective modulus D_{ijkl} is carried out only once before the solving of equation (6).

For the unidirectinal composite, the geometrical- and the material properties are invariant to translation along the axial direction y_3, as shown in Figure 2. We can thus specify the internal phase geometry by the geometrical information on the cross-section $\bar{Y}$ (see Figure 2); besides, the current problem is regarded as a generalized plane-strain problem. In this situation, we can consider the in-plane components χ^{kl}_β $(\beta = 1, 2)$ and the out-plane component χ^{kl}_3, separetely. The governing equations concerning $\boldsymbol{\chi}^{kl}$ are described by the following boundary integral equations [6][7]:

$$\begin{aligned} c_{\beta\gamma}\chi^{kl}_\gamma + \int_{\bar{S}} p^{(1)*}_{\beta\gamma} \chi^{kl}_\gamma \, d(\partial\bar{Y}_1) &= \int_{\bar{S}} u^{(1)*}_{\beta\gamma} \bar{p}^{(1)kl}_\gamma \, d(\partial\bar{Y}_1), \qquad (\text{for } \bar{Y}_1), \\ c_{\beta\gamma}\chi^{kl}_\gamma + \int_{\bar{S}+\bar{\Gamma}} p^{(2)*}_{\beta\gamma} \chi^{kl}_\gamma \, d(\partial\bar{Y}_2) &= \int_{\bar{S}+\bar{\Gamma}} u^{(2)*}_{\beta\gamma} \bar{p}^{(2)kl}_\gamma \, d(\partial\bar{Y}_2), \qquad (\text{for } \bar{Y}_2), \end{aligned} \tag{9}$$

for the in-plane components $(\beta = 1, 2)$, and

$$\begin{aligned} c\chi^{kl}_3 + \int_{\bar{S}} p^{(1)*}_{33} \chi^{kl}_3 \, d(\partial\bar{Y}_1) &= \int_{\bar{S}} u^{(1)*}_{33} \bar{p}^{(1)kl}_3 \, d(\partial\bar{Y}_1), \qquad (\text{for } \bar{Y}_1), \\ c\chi^{kl}_3 + \int_{\bar{S}+\bar{\Gamma}} p^{(2)*}_{33} \chi^{kl}_3 \, d(\partial\bar{Y}_2) &= \int_{\bar{S}+\bar{\Gamma}} u^{(2)*}_{33} \bar{p}^{(2)kl}_3 \, d(\partial\bar{Y}_2), \qquad (\text{for } \bar{Y}_2), \end{aligned} \tag{10}$$

for the out-plane component χ^{kl}_3. In equations (9) and (10), $\bar{S}$ is the interface of $\bar{Y}_1$ and $\bar{Y}_2$ in the cross-section $\bar{Y}$, and $\bar{\Gamma}$ is the outer boundary of $\bar{Y}$. $\bar{p}^{(\alpha)*}_j := E^{(\alpha)}_{ijpm} \chi^{kl}_{p,m} n^{(\alpha)}_i$. Moreover, $u^{(\alpha)*}_{\beta\gamma}$ and $p^{(\alpha)*}_{\beta\gamma}$ are the fundamental solutions of 2-D elastostatic ploblems, whereas $u^{(\alpha)*}_{33}$ and $p^{(\alpha)*}_{33}$ are given by

$$u^{(\alpha)*}_{33} := -\frac{1}{2\pi G^{(\alpha)}} \ln r, \qquad p^{(\alpha)*}_{33} := -\frac{1}{2\pi r} \frac{\partial r}{\partial n^{(\alpha)}}, \tag{11}$$

where r is the distance between the two points in the domain $\bar{Y}_\alpha$, and $G^{(\alpha)}$ is the shear modulus of the constituent $\bar{Y}_\alpha$. $n^{(\alpha)}$ denotes the outward normal direction on the boundary $\partial\bar{Y}_\alpha$.

On the other hand, the boundary conditions for calculating $\boldsymbol{\chi}^{kl}$ are described as follows:

$$\begin{aligned} \bar{p}_i^{(1)kl} + \bar{p}_i^{(2)kl} &= E_{ijkl}^{(1)} n_j^{(1)} + E_{ijkl}^{(2)} n_j^{(2)}, \qquad (\text{on } \bar{S}), \\ \boldsymbol{\chi}_{(left)}^{kl} = \boldsymbol{\chi}_{(right)}^{kl}, &\quad \boldsymbol{\chi}_{(top)}^{kl} = \boldsymbol{\chi}_{(bottom)}^{kl}, \quad (\text{on } \bar{\Gamma}), \\ \bar{\mathbf{p}}_{(left)}^{(2)kl} + \bar{\mathbf{p}}_{(right)}^{(2)kl} = \mathbf{0}, &\quad \bar{\mathbf{p}}_{(top)}^{(2)kl} + \bar{\mathbf{p}}_{(bottom)}^{(2)kl} = \mathbf{0}, \quad (\text{on } \bar{\Gamma}), \end{aligned} \tag{12}$$

where the subscripts "$(left)$", "$(right)$", "(top)" and "$(bottom)$" denote pieces of the boundary $\bar{\Gamma}$ of the cross-section $\bar{Y}$. For isotropic constituents, the force $E_{ijkl}^{(\alpha)} n_j^{(\alpha)}$ subjecting on $\bar{S}$ has alternatively the in-plane and out-plane components, which results from material isotropy and $n_3^{(\alpha)} = 0$. Hence, the out-plane components of $\boldsymbol{\chi}^{11}$, $\boldsymbol{\chi}^{22}$, $\boldsymbol{\chi}^{33}$ and $\boldsymbol{\chi}^{12}$, and the in-plane components of $\boldsymbol{\chi}^{23}$ and $\boldsymbol{\chi}^{31}$ vanish. In other words, we can simulate the responses of $\boldsymbol{\chi}^{11}$, $\boldsymbol{\chi}^{22}$, $\boldsymbol{\chi}^{33}$ and $\boldsymbol{\chi}^{12}$ through the in-plane analysis using equation (9), whereas $\boldsymbol{\chi}^{23}$ and $\boldsymbol{\chi}^{31}$ can be calculated by the out-plane analysis based on equation (10).

Like the simulation of the characteristic function $\boldsymbol{\chi}^{kl}$, we can evaluate the effective elastic modulus D_{ijkl} of the unidirectional composites only using the geometrical and material properties of the phase $\bar{Y}_\alpha$ [6], i.e.,

$$\begin{aligned} D_{ijkl} &= \frac{E_{ijkl}^{(1)} |\bar{Y}_1| + E_{ijkl}^{(2)} |\bar{Y}_2|}{|\bar{Y}|} - \frac{1}{|\bar{Y}|} \sum_{\alpha=1}^{2} \int_{\bar{S}} E_{ijpm}^{(\alpha)} \chi_p^{kl} n_m^{(\alpha)} \, d(\partial \bar{Y}_\alpha), \\ |\bar{Y}_\alpha| &= \int_{\bar{Y}_\alpha} d\bar{Y} = \frac{1}{2} \int_{\bar{S}} y_m n_m^{(\alpha)} \, d(\partial \bar{Y}_\alpha). \end{aligned} \tag{13}$$

3 Homogenization analysis using wavelet BEM

3.1. Assembly of boundary element equation

To evaluate the effective elastic moduli of unidirectional composites, we now utilize the wavelet BEM to numerically solve boundary integral equations (9) and (10) concerning the characteristic function $\boldsymbol{\chi}^{kl}$.

In the first stage of wavelet-based BE analysis, we need to discretize boundary integral equations (9) and (10). To achieve this, we introduce the approximate solutions $\tilde{\chi}_j^{kl}$ and $\tilde{\bar{p}}_j^{(\alpha)kl}$ defined as the wavelet series [17], i.e.,

$$\begin{aligned} \chi_j^{kl} \simeq \tilde{\chi}_j^{kl} &:= \sum_{p=1}^{n_s} \hat{X}_{j,p}^{kl} \phi_{0,p} + \sum_{m=0}^{M} \sum_{q=1}^{n_m} \tilde{X}_{j,mq}^{kl} \psi_{m,q}, \\ \bar{p}_j^{(\alpha)kl} \simeq \tilde{\bar{p}}_j^{(\alpha)kl} &:= \sum_{p=1}^{n_s} \hat{T}_{j,p}^{(\alpha)kl} \phi_{0,p} + \sum_{m=0}^{M} \sum_{q=1}^{n_m} \tilde{T}_{j,mq}^{(\alpha)kl} \psi_{m,q}, \end{aligned} \tag{14}$$

where $\phi_{0,p}$ and $\psi_{m,q}$ are the scaling function and the wavelet, respectively. In this study, we adopt the piecewise constant function and the Haar wavelet as $\phi_{0,p}$ and $\psi_{m,q}$. Thus,

$\phi_{0,p}$ and $\psi_{m,q}$ are defined by

$$\phi_{0,p} := \phi(\xi - p), \qquad \psi_{m,q} = 2^{\frac{m}{2}}\psi(2^m\xi - q), \tag{15}$$

$$\phi(\xi) := \begin{cases} 1, & 0 \le \xi \le 1, \\ 0, & \text{elsewhere}, \end{cases} \qquad \psi(\xi) := \begin{cases} 1, & 0 \le \xi \le 1/2, \\ -1, & 1/2 < \xi \le 1, \\ 0, & \text{elsewhere}. \end{cases} \tag{16}$$

Note that the wavelet ψ satisfies the first-order vanishing moment property as

$$\int_{-\infty}^{\infty} \psi(\xi) d\xi = 0. \tag{17}$$

In equation (14), $\hat{X}^{kl}_{j,p}$, $\tilde{X}^{kl}_{j,mq}$, $\hat{T}^{(\alpha)kl}_{j,p}$ and $\tilde{T}^{(\alpha)kl}_{j,mq}$ are the expansion coefficients of χ^{kl}_j and $\bar{p}^{(\alpha)kl}_j$. Moreover, M is the finest resolution level, and n_s and n_m are the numbers of the basis functions $\phi_{0,p}$ and $\psi_{m,q}$, respectively.

Substituting equation (14) into equations (9) and (10) and applying the Galerkin method to the resulting equation, we obtain the boundary element equations corresponding to the subdomains $\bar{Y}_1$ and $\bar{Y}_2$ as follows:

$$\mathbf{H}^{(1)}\mathbf{X}^{(1)kl}_{\bar{S}} = \mathbf{G}^{(1)}\mathbf{T}^{(1)kl}_{\bar{S}}, \tag{18}$$

$$\begin{aligned} &\begin{bmatrix} \mathbf{H}^{(2)}_{\bar{S},\bar{S}} & \mathbf{H}^{(2)}_{\bar{S},\bar{\Gamma}'} & \mathbf{H}^{(2)}_{\bar{S},\bar{\Gamma}'(opp)} \\ \mathbf{H}^{(2)}_{\bar{\Gamma}',\bar{S}} & \mathbf{H}^{(2)}_{\bar{\Gamma}',\bar{\Gamma}'} & \mathbf{H}^{(2)}_{\bar{\Gamma}',\bar{\Gamma}'(opp)} \\ \mathbf{H}^{(2)}_{\bar{\Gamma}'(opp),\bar{S}} & \mathbf{H}^{(2)}_{\bar{\Gamma}'(opp),\bar{\Gamma}'} & \mathbf{H}^{(2)}_{\bar{\Gamma}'(opp),\bar{\Gamma}'(opp)} \end{bmatrix} \begin{Bmatrix} \mathbf{X}^{(2)kl}_{\bar{S}} \\ \mathbf{X}^{kl}_{\bar{\Gamma}'} \\ \mathbf{X}^{kl}_{\bar{\Gamma}'(opp)} \end{Bmatrix} \\ &\qquad = \begin{bmatrix} \mathbf{G}^{(2)}_{\bar{S},\bar{S}} & \mathbf{G}^{(2)}_{\bar{S},\bar{\Gamma}'} & \mathbf{G}^{(2)}_{\bar{S},\bar{\Gamma}'(opp)} \\ \mathbf{G}^{(2)}_{\bar{\Gamma}',\bar{S}} & \mathbf{G}^{(2)}_{\bar{\Gamma}',\bar{\Gamma}'} & \mathbf{G}^{(2)}_{\bar{\Gamma}',\bar{\Gamma}'(opp)} \\ \mathbf{G}^{(2)}_{\bar{\Gamma}'(opp),\bar{S}} & \mathbf{G}^{(2)}_{\bar{\Gamma}'(opp),\bar{\Gamma}'} & \mathbf{G}^{(2)}_{\bar{\Gamma}'(opp),\bar{\Gamma}'(opp)} \end{bmatrix} \begin{Bmatrix} \mathbf{T}^{(2)kl}_{\bar{S}} \\ \mathbf{T}^{(2)kl}_{\bar{\Gamma}'} \\ \mathbf{T}^{(2)kl}_{\bar{\Gamma}'(opp)} \end{Bmatrix}. \end{aligned} \tag{19}$$

where $\mathbf{X}^{kl}$ and $\mathbf{T}^{(\alpha)kl}$ are the vectors of which components are the expasion coefficients in equation (14). The subscripts $\bar{S}$ and $\bar{\Gamma}$ stand for subboundaries on which the wavelet series $\tilde{\chi}^{kl}_j$ and $\tilde{\bar{p}}^{(\alpha)kl}_j$ are defined. Moreover, $\bar{\Gamma} = \bar{\Gamma}' \cup \bar{\Gamma}'_{(opp)}$ where $\bar{\Gamma}'_{(opp)}$ is the opposite side patch of the subboundaries $\bar{\Gamma}'$. In assembly of the boundary element equation, we will impose the displacement continuity and traction equilibrium conditions induced by spatial periodicity of the microstructures on the expansion coefficients $\mathbf{X}^{kl}_{\bar{\Gamma}'}$, $\mathbf{X}^{kl}_{\bar{\Gamma}'(opp)}$, $\mathbf{T}^{(\alpha)kl}_{\bar{\Gamma}'}$ and $\mathbf{T}^{(\alpha)kl}_{\bar{\Gamma}'(opp)}$ on the subboundaries $\bar{\Gamma}'$ and $\bar{\Gamma}'_{(opp)}$, as has been shown in equation (12). Furthermore, the coefficient matrices $\mathbf{G}^{(\alpha)}$ and $\mathbf{H}^{(\alpha)}$ have the following elements $g^{(\alpha)}_{(p,q)(i,j)}$ and $h^{(\alpha)}_{(p,q)(i,j)}$:

$$\begin{aligned} g^{(\alpha)}_{(p,q)(i,j)} &:= \int_{\partial Y_\alpha} w_p \int_{\partial Y_\alpha} u^{(\alpha)*}_{ij} w_q \, d(\partial Y_\alpha)^2, \\ h^{(\alpha)}_{(p,q)(i,j)} &:= \frac{1}{2}\delta_{ij} \int_{\partial Y_\alpha} w_p w_q \, d(\partial Y_\alpha) + \int_{\partial Y_\alpha} w_p \int_{\partial Y_\alpha} p^{(\alpha)*}_{ij} w_q \, d(\partial Y_\alpha)^2, \end{aligned} \tag{20}$$

$$\begin{aligned} \{w_p \,|p = 1, \ldots, N\} := \{&\phi_{0,\beta},\ \phi_{m,\gamma} \,| \quad \beta = 1, \ldots, n_s, \\ &m = 0, \ldots, M,\ \gamma = 1, \ldots, n_m(m)\}, \end{aligned}$$

where $u_{\beta 3}^{(\alpha)*} = u_{3\beta}^{(\alpha)*} = 0$ and $p_{\beta 3}^{(\alpha)*} = p_{3\beta}^{(\alpha)*} = 0$ for $\beta = 1, 2$.

Secondary, let us consider the continuity of the characteristic function $\boldsymbol{\chi}^{kl}$ and the equilibrium of the traction $\bar{\mathbf{p}}^{(\alpha)kl}$. In this case, the displacement continuity and traction equilibrium conditions are derived from equation (12) as follows:

$$
\begin{aligned}
&\mathbf{X}_{\bar{S}}^{(1)kl} = \boldsymbol{\rho}_{\bar{S}} \mathbf{X}_{\bar{S}}^{(2)kl}, \qquad \mathbf{T}_{\bar{S}}^{(1)kl} + \boldsymbol{\rho}_{\bar{S}} \mathbf{T}_{\bar{S}}^{(2)kl} = \mathbf{F}, \\
&\mathbf{X}_{\bar{\Gamma}'(opp)}^{kl} = \boldsymbol{\rho}_{\bar{\Gamma}'} \mathbf{X}_{\bar{\Gamma}'}^{kl}, \qquad \mathbf{T}_{\bar{\Gamma}'(opp)}^{(2)kl} + \boldsymbol{\rho}_{\bar{\Gamma}'} \mathbf{T}_{\bar{\Gamma}'}^{(2)kl} = \mathbf{0}, \\
&\boldsymbol{\rho}_{\bar{S}} = \{\rho_\beta \delta_{\beta\zeta} \mid \beta = 1, \ldots, 3N_s\} \in \mathbb{R}^{3N_s \times 3N_s}, \\
&\boldsymbol{\rho}_{\bar{\Gamma}'} = \{\rho_\gamma \delta_{\gamma\zeta} \mid \gamma = 1, \ldots, \frac{3}{2}(N - N_s)\} \in \mathbb{R}^{\frac{3}{2}(N-N_s) \times \frac{3}{2}(N-N_s)},
\end{aligned}
\tag{21}
$$

where N_s is the number of basis functions used for the interpolation on the interface $\bar{S}$. The known vector $\mathbf{F}$ has the components given by the expansion coefficients of the force $E_{ijkl}^{(1)} n_j^{(1)} + E_{ijkl}^{(2)} n_j^{(2)}$ subjecting on $\bar{S}$. Moreover, ρ_β is set either to 1 (w_β: scaling function) or -1 (w_β: wavelet), which is available only for the Haar wavelets. If other wavelets are employed as the basis functions in the analysis, we will have to determine ρ_β in consideration of the symmetry and asymmetry of the basis functions.

Now, imposing restriction (21) on boundary element equations (18) and (19), we obtain a system of algebraic equations with unknowns $\mathbf{X}_{\bar{S}}^{(2)kl}$, $\mathbf{X}_{\bar{\Gamma}'}^{kl}$, $\mathbf{T}_{\bar{S}}^{(2)kl}$ and $\mathbf{T}_{\bar{\Gamma}'}^{(2)kl}$ as follows:

$$
\begin{bmatrix}
\boldsymbol{\rho}_{\bar{S}} \mathbf{H}^{(1)} & \boldsymbol{\rho}_{\bar{S}} \mathbf{G}^{(1)} & \mathbf{0} \\
\mathbf{H}_{\bar{S},\bar{S}}^{(2)} & -\mathbf{G}_{\bar{S},\bar{S}}^{(2)} & \mathbf{H}_{\bar{S},\bar{\Gamma}'}^{(2)} + \boldsymbol{\rho}_{\bar{\Gamma}'} \mathbf{H}_{\bar{S},\bar{\Gamma}'(opp)}^{(2)} \\
\mathbf{H}_{\bar{\Gamma}',\bar{S}}^{(2)} & -\mathbf{G}_{\bar{\Gamma}',\bar{S}}^{(2)} & \mathbf{H}_{\bar{\Gamma}',\bar{\Gamma}'}^{(2)} + \boldsymbol{\rho}_{\bar{\Gamma}'} \mathbf{H}_{\bar{\Gamma}',\bar{\Gamma}'(opp)}^{(2)} \\
\mathbf{H}_{\bar{\Gamma}'(opp),\bar{S}}^{(2)} & -\mathbf{G}_{\bar{\Gamma}'(opp),\bar{S}}^{(2)} & \mathbf{H}_{\bar{\Gamma}'(opp),\bar{\Gamma}'}^{(2)} + \boldsymbol{\rho}_{\bar{\Gamma}'} \mathbf{H}_{\bar{\Gamma}'(opp),\bar{\Gamma}'(opp)}^{(2)}
\end{bmatrix}
\begin{bmatrix}
\mathbf{0} \\
-(\mathbf{G}_{\bar{S},\bar{\Gamma}'}^{(2)} - \boldsymbol{\rho}_{\bar{\Gamma}'} \mathbf{G}_{\bar{S},\bar{\Gamma}'(opp)}^{(2)}) \\
-(\mathbf{G}_{\bar{\Gamma}',\bar{\Gamma}'}^{(2)} - \boldsymbol{\rho}_{\bar{\Gamma}'} \mathbf{G}_{\bar{\Gamma}',\bar{\Gamma}'(opp)}^{(2)}) \\
-(\mathbf{G}_{\bar{\Gamma}'(opp),\bar{\Gamma}'}^{(2)} - \boldsymbol{\rho}_{\bar{\Gamma}'} \mathbf{G}_{\bar{\Gamma}'(opp),\bar{\Gamma}'(opp)}^{(2)})
\end{bmatrix}
\begin{Bmatrix}
\mathbf{X}_{\bar{S}}^{(2)kl} \\ \mathbf{T}_{\bar{S}}^{(2)kl} \\ \mathbf{X}_{\bar{\Gamma}'}^{kl} \\ \mathbf{T}_{\bar{\Gamma}'}^{(2)kl}
\end{Bmatrix}
=
\begin{Bmatrix}
\mathbf{G}^{(1)}\mathbf{F} \\ \mathbf{0} \\ \mathbf{0} \\ \mathbf{0}
\end{Bmatrix}.
\tag{22}
$$

In equation (22), the coefficient matrix is singular, since the translation of the unit cell is not quite restricted by boundary conditions (12). We can however, calculate one of the non-unique solutions including the translation modes, using an iterative solver that has a residual-based termination algorithm for the iterative process. Then, we have no need to regularize simultaneous equation (22). This results from as follows: the initial guess used in the iterative process prescribes the rigid body motion of the cell and the translation modes in the iterative solution do not affect the residual norm used for the decision of iteration termination. In the present approach for homogenization analysis, we can straightforwardly use the BE solution $\tilde{\boldsymbol{\chi}}^{kl}$ including the translation modes to evaluate the effective elastic moduli of unidirectional composites. The translation components in $\tilde{\boldsymbol{\chi}}^{kl}$ obviously depends on the setting of the initial guess; however, the effective elastic modulus evaluated by equation (13) is independent of the quantity of translation of the unit cell. We can easily prove the translation independency of D_{ijkl} using definition (7) of D_{ijkl} and the divergence theorem.

3.2. Rearrangement of boundary element equation for rapid convergence of iterative solution

As mentioned above, an iterative solver is used to calculate the BE solution $\tilde{\boldsymbol{\chi}}^{kl}$ of the characteristic function with equation (22). This is because in wavelet-based BE analysis the system matrix of boundary element equations becomes sparse and no regularization of the equation is required. To save the computation time for solving the equation, it is essential to attain convergence in the iterative solutions with less number of iterations. In general, the computational work required up to termination of the iteration depends not only on the number of non-zero entries, but also on the population of coefficient matrix entries. For the homogenization analysis with the wavelet BEM, the dominant entries of the coefficient matrix of equation (22) are not concentrated in the vicinity of matrix diagonal. This may incur the increase in the number of iterations. To avoid increasing the computational work for the iteration, we now propose a special preconditioning algorithm: the rearrangement of simultaneous equation (22).

Let us now consider the boundary element equation given by equation (22). This equation can be described symbolically as

$$\begin{bmatrix} \mathbf{A}_{11} & \mathbf{A}_{12} & \mathbf{A}_{13} & \mathbf{A}_{14} \\ \mathbf{A}_{21} & \mathbf{A}_{22} & \mathbf{A}_{23} & \mathbf{A}_{24} \\ \mathbf{A}_{31} & \mathbf{A}_{32} & \mathbf{A}_{33} & \mathbf{A}_{34} \\ \mathbf{A}_{41} & \mathbf{A}_{42} & \mathbf{A}_{43} & \mathbf{A}_{44} \end{bmatrix} \begin{Bmatrix} \mathbf{z}_1 \\ \mathbf{z}_2 \\ \mathbf{z}_3 \\ \mathbf{z}_4 \end{Bmatrix} = \begin{Bmatrix} \mathbf{b}_1 \\ \mathbf{b}_2 \\ \mathbf{b}_3 \\ \mathbf{b}_4 \end{Bmatrix}. \tag{23}$$

Besides, it is assumed that the rearrangement of equation (23) yields the resulting equation as

$$\begin{bmatrix} \mathbf{A}'_{11} & \mathbf{A}'_{12} & \mathbf{A}'_{13} & \mathbf{A}'_{14} \\ \mathbf{A}'_{21} & \mathbf{A}'_{22} & \mathbf{A}'_{23} & \mathbf{A}'_{24} \\ \mathbf{A}'_{31} & \mathbf{A}'_{32} & \mathbf{A}'_{33} & \mathbf{A}'_{34} \\ \mathbf{A}'_{41} & \mathbf{A}'_{42} & \mathbf{A}'_{43} & \mathbf{A}'_{44} \end{bmatrix} \begin{Bmatrix} \mathbf{z}'_1 \\ \mathbf{z}'_2 \\ \mathbf{z}'_3 \\ \mathbf{z}'_4 \end{Bmatrix} = \begin{Bmatrix} \mathbf{b}'_1 \\ \mathbf{b}'_2 \\ \mathbf{b}'_3 \\ \mathbf{b}'_4 \end{Bmatrix}. \tag{24}$$

In the present study, we reconstruct equation (23) based on the following rule, in order to guarantee the nearly diagonal dominance of the coefficient matrix:

$$\begin{aligned} \mathbf{A}'_{2i-1,j} &\longleftarrow \mathbf{A}_{2i-1,j} + \boldsymbol{\rho}_i \mathbf{A}_{2i,j}, \\ \mathbf{A}'_{2i,j} &\longleftarrow \mathbf{A}_{2i-1,j} - \boldsymbol{\rho}_i \mathbf{A}_{2i,j}, \end{aligned} \qquad \mathbf{z}'_j \longleftarrow \mathbf{z}_j, \qquad \begin{aligned} \mathbf{b}'_{2i-1} &\longleftarrow \mathbf{b}_{2i-1} + \boldsymbol{\rho}_i \mathbf{b}_{2i}, \\ \mathbf{b}'_{2i} &\longleftarrow \mathbf{b}_{2i-1} - \boldsymbol{\rho}_i \mathbf{b}_{2i}, \end{aligned} \tag{25}$$

where $i = 1, 2$, $j = 1, 2, 3, 4$ and $\boldsymbol{\rho}$ is a diagonal matrix.

We now apply rearrangement rule (25) to boundary element equation (22) and choose $\boldsymbol{\rho}_1 = \boldsymbol{\rho}_{\bar{S}}^T = \boldsymbol{\rho}_{\bar{S}}$ and $\boldsymbol{\rho}_2 = \boldsymbol{\rho}_{\bar{\Gamma}'}^T = \boldsymbol{\rho}_{\bar{\Gamma}'}$. As a result, we obtain the resulting simultaneous

equation as follows:

$$
\left[\begin{array}{cc}
\boldsymbol{\rho}_{\bar{S}}(\mathbf{H}^{(1)}+\mathbf{H}^{(2)}_{\bar{S},\bar{S}}) & \boldsymbol{\rho}_{\bar{S}}(\mathbf{G}^{(1)}-\mathbf{G}^{(2)}_{\bar{S},\bar{S}}) \\
\boldsymbol{\rho}_{\bar{S}}(\mathbf{H}^{(1)}-\mathbf{H}^{(2)}_{\bar{S},\bar{S}}) & \boldsymbol{\rho}_{\bar{S}}(\mathbf{G}^{(1)}+\mathbf{G}^{(2)}_{\bar{S},\bar{S}}) \\
\mathbf{H}^{(2)}_{\bar{\Gamma}',\bar{S}}+\boldsymbol{\rho}_{\bar{\Gamma}'}\mathbf{H}^{(2)}_{\bar{\Gamma}'(opp),\bar{S}} & -\mathbf{G}^{(2)}_{\bar{\Gamma}',\bar{S}}-\boldsymbol{\rho}_{\bar{\Gamma}'}\mathbf{G}^{(2)}_{\bar{\Gamma}'(opp),\bar{S}} \\
\mathbf{H}^{(2)}_{\bar{\Gamma}',\bar{S}}-\boldsymbol{\rho}_{\bar{\Gamma}'}\mathbf{H}^{(2)}_{\bar{\Gamma}'(opp),\bar{S}} & -\mathbf{G}^{(2)}_{\bar{\Gamma}',\bar{S}}+\boldsymbol{\rho}_{\bar{\Gamma}'}\mathbf{G}^{(2)}_{\bar{\Gamma}'(opp),\bar{S}}
\end{array}\right.
$$

$$
\left.\begin{array}{cc}
\boldsymbol{\rho}_{\bar{S}}(\mathbf{H}^{(2)}_{\bar{S},\bar{\Gamma}'}+\boldsymbol{\rho}_{\bar{\Gamma}'}\mathbf{H}^{(2)}_{\bar{S},\bar{\Gamma}'(opp)}) & -\boldsymbol{\rho}_{\bar{S}}(\mathbf{G}^{(2)}_{\bar{S},\bar{\Gamma}'}-\boldsymbol{\rho}_{\bar{\Gamma}'}\mathbf{G}^{(2)}_{\bar{S},\bar{\Gamma}'(opp)}) \\
-\boldsymbol{\rho}_{\bar{S}}(\mathbf{H}^{(2)}_{\bar{S},\bar{\Gamma}'}+\boldsymbol{\rho}_{\bar{\Gamma}'}\mathbf{H}^{(2)}_{\bar{S},\bar{\Gamma}'(opp)}) & \boldsymbol{\rho}_{\bar{S}}(\mathbf{G}^{(2)}_{\bar{S},\bar{\Gamma}'}-\boldsymbol{\rho}_{\bar{\Gamma}'}\mathbf{G}^{(2)}_{\bar{S},\bar{\Gamma}'(opp)}) \\
\mathbf{H}^{(2)}_{\bar{\Gamma}',\bar{\Gamma}'}+\boldsymbol{\rho}_{\bar{\Gamma}'}\mathbf{H}^{(2)}_{\bar{\Gamma}',\bar{\Gamma}'(opp)}+\boldsymbol{\rho}_{\bar{\Gamma}'}(\mathbf{H}^{(2)}_{\bar{\Gamma}'(opp),\bar{\Gamma}'}+\boldsymbol{\rho}_{\bar{\Gamma}'}\mathbf{H}^{(2)}_{\bar{\Gamma}'(opp),\bar{\Gamma}'(opp)}) & -(\mathbf{G}^{(2)}_{\bar{\Gamma}',\bar{\Gamma}'}-\boldsymbol{\rho}_{\bar{\Gamma}'}\mathbf{G}^{(2)}_{\bar{\Gamma}',\bar{\Gamma}'(opp)})-\boldsymbol{\rho}_{\bar{\Gamma}'}(\mathbf{G}^{(2)}_{\bar{\Gamma}'(opp),\bar{\Gamma}'}-\boldsymbol{\rho}_{\bar{\Gamma}'}\mathbf{G}^{(2)}_{\bar{\Gamma}'(opp),\bar{\Gamma}'(opp)}) \\
\mathbf{H}^{(2)}_{\bar{\Gamma}',\bar{\Gamma}'}+\boldsymbol{\rho}_{\bar{\Gamma}'}\mathbf{H}^{(2)}_{\bar{\Gamma}',\bar{\Gamma}'(opp)}-\boldsymbol{\rho}_{\bar{\Gamma}'}(\mathbf{H}^{(2)}_{\bar{\Gamma}'(opp),\bar{\Gamma}'}+\boldsymbol{\rho}_{\bar{\Gamma}'}\mathbf{H}^{(2)}_{\bar{\Gamma}'(opp),\bar{\Gamma}'(opp)}) & -(\mathbf{G}^{(2)}_{\bar{\Gamma}',\bar{\Gamma}'}-\boldsymbol{\rho}_{\bar{\Gamma}'}\mathbf{G}^{(2)}_{\bar{\Gamma}',\bar{\Gamma}'(opp)})+\boldsymbol{\rho}_{\bar{\Gamma}'}(\mathbf{G}^{(2)}_{\bar{\Gamma}'(opp),\bar{\Gamma}'}-\boldsymbol{\rho}_{\bar{\Gamma}'}\mathbf{G}^{(2)}_{\bar{\Gamma}'(opp),\bar{\Gamma}'(opp)})
\end{array}\right]
\left\{\begin{array}{c}
\mathbf{X}^{(2)kl}_{\bar{S}} \\
\mathbf{T}^{(2)kl}_{\bar{S}} \\
\mathbf{X}^{kl}_{\bar{\Gamma}'} \\
\mathbf{T}^{(2)kl}_{\bar{\Gamma}'}
\end{array}\right\}
=
\left\{\begin{array}{c}
\mathbf{G}^{(1)}\mathbf{F} \\
\mathbf{G}^{(1)}\mathbf{F} \\
\mathbf{0} \\
\mathbf{0}
\end{array}\right\}. \tag{26}
$$

In equation (26), all the diagonal blocks of the coefficient matrix include additions of the diagonal blocks of original boundary element equations (18) and (19), and thus the additions may not vanish independently of the components of $\boldsymbol{\rho}_{\bar{S}}$ and $\boldsymbol{\rho}_{\bar{\Gamma}'}$. On the other hand, the off-diagonal blocks are constructed by subtractions of the diagonal blocks in the original equations and additions of the off-diagonal blocks in equations (18) and (19). Hence, it is expected that the off-diagonal blocks in equation (26) have smaller entries than those of the diagonal blocks. The resulting equation (26) has the coefficient matrix with nearly diagonal dominance, which will ensure the rapid convergence of iterative solutions. In the below, we use equation (26) to evaluate the characteristic functions $\boldsymbol{\chi}^{kl}$. The proposed approach will be validated in Section 4.

3.3. Matrix compression scheme

In the wavelet-based BE analysis, we can enhance the computational performance by matrix compression, i.e., generating a sparse matrix of boundary element equations. The sparse matrix is yielded by the truncation of its small entries. In this study, the truncation of the matrix entries is carried out using the Beylkin-type algorithm [11].

The Matrix compression based on Beylkin-type algorithm is very simple; besides we can determine the optimal thresholding value for this algorithm as proposed in Ref.[18]. To save the computational work, the truncation before generation of the entries — *a priori* truncation — is carried out together with *a posteriori* truncation.

In assembly of the coefficient matrix, we first estimate approximations G_{est} and H_{est} for every entry, prior to the calculation of equation (20). The *a priori* estimations G_{est} and H_{est} are given to every submatrix concerning a certain combination of the basis functions w_p and w_q, for the sake of simplicity of the algorithm. Besides, they are generated in consideration of the periodicity conditions of the unit cell in order to avoid overtruncation.

If *a priori* estimations G_{est} and H_{est} satisfy the following truncation criteria:

$$G_{est} < \tau \cdot G_{max}, \qquad H_{est} < \tau \cdot H_{max}, \tag{27}$$

then, the entries are regarded as zero and they are truncated without calculation of equation (20). In criterion (27), G_{max} and H_{max} are the representative values of the matrix coefficients $|g^{(\alpha)}_{(p,q)(i,j)}|$ and $|h^{(\alpha)}_{(p,q)(i,j)}|$, respectively. Moreover, τ is the optimal threshold parameter, and its value is determined by the practical strategy developed by the authors [18]. Justification of the present strategy will be verified in the next section.

G_{est} and H_{est} are generated by derivative-type estimation; however, this approach is not straightforwardly applied to the BE-based homogenization analysis. This is because we need to impose the periodicity conditions of the unit cell on boundary element equations (18) and (19) and to implement the rearrangement algorithm to attain the termination of the iterative process with less computational work. Since the setting of such estimations to inappropriate values incurs overtruncation under certain circumstances, we define *a priori* estimations G_{est} and H_{est} as follows:

$$G_{est} := \begin{cases} \bar{g}^{(\alpha)}_{w_p,w_q}, & (\text{supp } w_p \in S,\ \text{supp } w_q \in S) \\ \bar{g}^{(\alpha)}_{w_p,w_q} + \bar{g}^{(\alpha)}_{w_p,w_{q(opp)}}, & (\text{supp } w_p \in S,\ \text{supp } w_q \in \Gamma) \\ \bar{g}^{(\alpha)}_{w_p,w_q} + \bar{g}^{(\alpha)}_{w_{p(opp)},w_q}, & (\text{supp } w_p \in \Gamma,\ \text{supp } w_q \in S) \\ \bar{g}^{(\alpha)}_{w_p,w_q} + \bar{g}^{(\alpha)}_{w_p,w_{q(opp)}} & \\ \qquad +\bar{g}^{(\alpha)}_{w_{p(opp)},w_q} + \bar{g}^{(\alpha)}_{w_{p(opp)},w_{q(opp)}}, & (\text{supp } w_p \in \Gamma,\ \text{supp } w_q \in \Gamma) \end{cases} \tag{28}$$

$$H_{est} := \begin{cases} \bar{h}^{(\alpha)}_{w_p,w_q}, & (\text{supp } w_p \in S,\ \text{supp } w_q \in S) \\ \bar{h}^{(\alpha)}_{w_p,w_q} + \bar{h}^{(\alpha)}_{w_p,w_{q(opp)}}, & (\text{supp } w_p \in S,\ \text{supp } w_q \in \Gamma) \\ \bar{h}^{(\alpha)}_{w_p,w_q} + \bar{h}^{(\alpha)}_{w_{p(opp)},w_q}, & (\text{supp } w_p \in \Gamma,\ \text{supp } w_q \in S) \\ \bar{h}^{(\alpha)}_{w_p,w_q} + \bar{h}^{(\alpha)}_{w_p,w_{q(opp)}} & \\ \qquad +\bar{h}^{(\alpha)}_{w_{p(opp)},w_q} + \bar{h}^{(\alpha)}_{w_{p(opp)},w_{q(opp)}}, & (\text{supp } w_p \in \Gamma,\ \text{supp } w_q \in \Gamma) \end{cases} \tag{29}$$

where $\bar{g}^{(\alpha)}_{(w_p,w_q)}$ and $\bar{h}^{(\alpha)}_{(w_p,w_q)}$ are approximate values of $|g^{(\alpha)}_{(p,q)(i,j)}|$ and $|h^{(\alpha)}_{(p,q)(i,j)}|$ that are esimated by the derivative-type approach, and they represent the magnitude of the entries in the submatrices $\{g^{(\alpha)}_{(p,q)(i,j)} | i,j = 1,2\}$ and $\{h^{(\alpha)}_{(p,q)(i,j)} | i,j = 1,2\}$ for the in-plane analysis, and of the entries $g^{(\alpha)}_{(p,q)(3,3)}$ and $h^{(\alpha)}_{(p,q)(3,3)}$ for the out-plane analysis.

On the other hand, the matrix entries over a fixed thresholding value are calculated by equation (20). When the matrix elements $g^{(\alpha)}_{(p,q)(i,j)}$ and $h^{(\alpha)}_{(p,q)(i,j)}$ hold the following inequalities:

$$|G^{(\alpha)}_{(p,q)(i,j)}| < \tau G_{max}, \qquad |H^{(\alpha)}_{(p,q)(i,j)}| < \tau H_{max}, \tag{30}$$

then, these entries are truncated *a posteriori*. In inequality (30), $G^{(\alpha)}_{(p,q)(i,j)}$ and $H^{(\alpha)}_{(p,q)(i,j)}$ are the matrix entries of equation (26), and correspond to the entries $g^{(\alpha)}_{(p,q)(i,j)}$ and $h^{(\alpha)}_{(p,q)(i,j)}$ generated by double integrals concerning the kernel functions $u^{(\alpha)*}_{ij}$ and $p^{(\alpha)*}_{ij}$, respectively.

In the present study, the truncation of small matrix entries is carried out to equation (26) with the periodicity conditions and the rearrangements. However, we can also make a sparse system of boundary element equation by application of the present compression scheme to equations (18) and (19). The validity of this strategy and the influence of the present compression schemes on the computational performance will be examined through numerical experiments in the next section.

4 Numerical results

In the preceding section, we have attempted to develop a wavelet BEM that shows high computational performance in the homogenization analysis. To achieve it, we have proposed two strategies: the rearrangement of boundary element equations and the matrix compression strategy. In this section, we will verify the availability of such strategies. Furthermore, the behavior of errors of the effective elastic moduli will be investigated through numerical experiments.

4.1. Problem descriptions

In the present study, we adopted unidirectional composites with 4 kinds of microstructures as the test examples. The geometrical profiles of these examples are shown in Figure 4. The unit cells in these examples are given as unit squares in every case, and the circular voids with radii $R_1 = 1/6$, $R_2 = 1/18$ and $R_3 = 1/54$ or the rectangular voids with sizes $L_1 = 1/3$, $L_2 = 1/9$ and $L_3 = 1/27$ are embedded in the matrix (Young's modulus: $E^{(2)} = 1$, Poisson's ratio: $\nu^{(2)} = 0.3$). We now discuss the characteristic functions $\boldsymbol{\chi}^{11}$, $\boldsymbol{\chi}^{22}$, $\boldsymbol{\chi}^{33}$ and $\boldsymbol{\chi}^{12}$ that have only the in-plane components. Then, we can evaluate 7 independent components of the effective elastic moduli excepting D_{2323} and D_{3131}.

As mentioned above, four kinds of the characteristic functions — $\boldsymbol{\chi}^{11}$, $\boldsymbol{\chi}^{22}$, $\boldsymbol{\chi}^{33}$ and $\boldsymbol{\chi}^{12}$ — are calculated using the wavelet BEM for 2-D elastostatic problems. Then, the boundary element equations concerning $\boldsymbol{\chi}^{kl}$ are derived for a matrix phase with voids as follows:

$$
\begin{bmatrix}
\mathbf{H}_{\bar{S},\bar{S}} & \mathbf{H}_{\bar{S},\bar{\Gamma}'} + \boldsymbol{\rho}_{\Gamma'}\mathbf{H}_{\bar{S},\bar{\Gamma}'(opp)} & -(\mathbf{G}_{\bar{S},\bar{\Gamma}'} - \boldsymbol{\rho}_{\Gamma'}\mathbf{G}_{\bar{S},\bar{\Gamma}'(opp)}) \\
\mathbf{H}_{\bar{\Gamma}',\bar{S}} + \boldsymbol{\rho}_{\Gamma'}\mathbf{H}_{\bar{\Gamma}'(opp),\bar{S}} & (\mathbf{H}_{\bar{\Gamma}',\bar{\Gamma}'} + \boldsymbol{\rho}_{\Gamma'}\mathbf{H}_{\bar{\Gamma}',\bar{\Gamma}'(opp)}) + \boldsymbol{\rho}_{\Gamma'}(\mathbf{H}_{\bar{\Gamma}'(opp),\bar{\Gamma}'} + \boldsymbol{\rho}_{\Gamma'}\mathbf{H}_{\bar{\Gamma}'(opp),\bar{\Gamma}'(opp)}) & -(\mathbf{G}_{\bar{\Gamma}',\bar{\Gamma}'} - \boldsymbol{\rho}_{\Gamma'}\mathbf{G}_{\bar{\Gamma}',\bar{\Gamma}'(opp)}) - \boldsymbol{\rho}_{\Gamma'}(\mathbf{G}_{\bar{\Gamma}'(opp),\bar{\Gamma}'} - \boldsymbol{\rho}_{\Gamma'}\mathbf{G}_{\bar{\Gamma}'(opp),\bar{\Gamma}'(opp)}) \\
\mathbf{H}_{\bar{\Gamma}',\bar{S}} - \boldsymbol{\rho}_{\Gamma'}\mathbf{H}_{\bar{\Gamma}'(opp),\bar{S}} & (\mathbf{H}_{\bar{\Gamma}',\bar{\Gamma}'} + \boldsymbol{\rho}_{\Gamma'}\mathbf{H}_{\bar{\Gamma}',\bar{\Gamma}'(opp)}) - \boldsymbol{\rho}_{\Gamma'}(\mathbf{H}_{\bar{\Gamma}'(opp),\bar{\Gamma}'} + \boldsymbol{\rho}_{\Gamma'}\mathbf{H}_{\bar{\Gamma}'(opp),\bar{\Gamma}'(opp)}) & -(\mathbf{G}_{\bar{\Gamma}',\bar{\Gamma}'} - \boldsymbol{\rho}_{\Gamma'}\mathbf{G}_{\bar{\Gamma}',\bar{\Gamma}'(opp)}) + \boldsymbol{\rho}_{\Gamma'}(\mathbf{G}_{\bar{\Gamma}'(opp),\bar{\Gamma}'} - \boldsymbol{\rho}_{\Gamma'}\mathbf{G}_{\bar{\Gamma}'(opp),\bar{\Gamma}'(opp)})
\end{bmatrix}
\begin{Bmatrix}
\mathbf{X}^{kl}_{\bar{S}} \\ \mathbf{X}^{kl}_{\bar{\Gamma}'} \\ \mathbf{T}^{kl}_{\bar{\Gamma}'}
\end{Bmatrix}
=
\begin{Bmatrix}
\mathbf{G}_{\bar{S},\bar{S}}\mathbf{T}_{\bar{S}} \\ \mathbf{G}_{\bar{\Gamma}',\bar{S}}\mathbf{T}_{\bar{S}} \\ \mathbf{G}_{\bar{\Gamma}'(opp),\bar{S}}\mathbf{T}_{\bar{S}}
\end{Bmatrix}.
\tag{31}
$$

where $\mathbf{T}_{\bar{S}}$ is the known vector of which components are given by expansion coefficients of the force $E^{(2)}_{ijkl}n^{(2)}_j$ on the boundary $\bar{S}$. In this study, linear algebraic equation (31) is

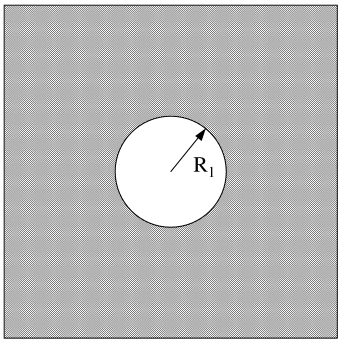

(a) Ex.1.

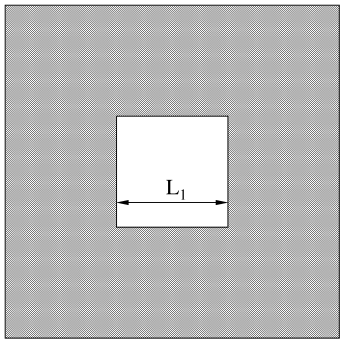

(b) Ex.2.

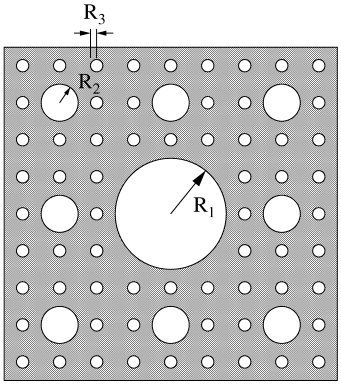

(c) Ex.3.

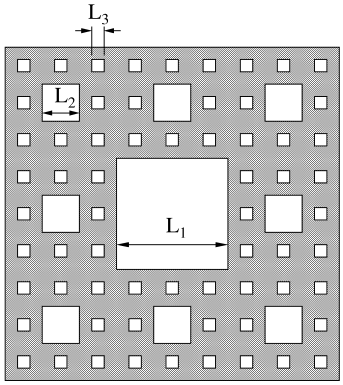

(d) Ex.4.

Figure 4: Unit cells in the present numerical tests. (Radii of circular voids: $R_1 = 1/6$, $R_2 = 1/18$ and $R_3 = 1/54$, sizes of rectangular voids: $L_1 = 1/3$, $L_2 = 1/9$ and $L_3 = 1/27$)

constructed using Haar wavelets. It follows that the matrix $\boldsymbol{\rho}_{\Gamma'}$ is defined by

$$\boldsymbol{\rho}_{\Gamma'} = \{\rho_{(p,q)(i,j)}\} = \begin{cases} 1, & (p = q,\ i = j,\ w_p = \phi), \\ -1, & (p = q,\ i = j,\ w_p = \psi), \\ 0, & (\text{otherwise}), \end{cases} \tag{32}$$

where $p, q = 1, \ldots, (N - N_s)/2$ and $i, j = 1, 2$. $\boldsymbol{\rho}_{\Gamma'}$ is a diagonal matrix, and hence $\boldsymbol{\rho}_{\Gamma'}^T = \boldsymbol{\rho}_{\Gamma'}$.

4.2. Numerical approach of singular and nearly-singular integrals

In assembly of equation (31), we have to calculate double integrals (20) on the boundaries $\bar{S}$ and $\bar{\Gamma}'$. Through this calculation, we generate the coefficient matrix entries using a hybrid scheme of analytical integration and the wavelet-weighted quadrature formulae proposed in Ref. [19]. The analytical integration scheme is applied to the integral on a straight line in the case of 2-D elastostatic problems. On the other hand, the numerical integration scheme, in which the wavelet-weighted formulae are adopted, is used to calculate another-type integrals in the current examples. Then, the numerical integration without

any regularization and smoothing of the kernel functions causes the accuracy reduction of the singular- and nearly singular integrals. We hence calculate these integrals using the wavelet-weighted formulae with the subtraction approach [20][21], and will consequently prevent the accuracy reduction.

Let us first consider a double integral with a singular kernel defined as:

$$I_{(p,q)} := \int_{-h_x/2}^{h_x/2} w_p(\xi) \int_{-h_y/2}^{h_y/2} K(\xi,\eta) w_q(\eta) J_q(\eta) d\eta \; J_p(\xi) d\xi, \tag{33}$$

where the kernel function $K(\xi,\eta)$ is given by $\ln r(\xi,\eta)$ or $\frac{1}{r}\frac{\partial r}{\partial s}$. $J_p(\xi) = d\Gamma/d\xi$ and $J_q(\eta) = d\Gamma/d\eta$, and w_p and w_q are basis functions. Moreover, it is assumed that supp $w_p = [-h_x/2, h_x/2]$ and supp $w_q = [-h_y/2, h_y/2]$.

In the present examples, we need to deal with a singular integral on a circular arc, and then $J_p(\xi)$ and $J_q(\eta)$ are constants $\bar{J}_p$ and $\bar{J}_q$, respectively. That is,

$$I_{(p,q)} := \bar{J}_p \bar{J}_q \int_{-h_x/2}^{h_x/2} w_p(\xi) \int_{-h_y/2}^{h_y/2} K(\xi,\eta) w_q(\eta) d\eta \; d\xi, \tag{34}$$

We now isolate a singular term K_s included in the original integrand K as follows:

$$K = (K - K_s) + K_s. \tag{35}$$

In this study, K_s is given by the asymptotical expansion of the singular kernel K around a singular point η_0 on the intrinsic coordinate η as

$$K_s = \begin{cases} \ln \bar{J}_q |\eta - \eta_0|, & (K = \ln r), \\ \dfrac{1}{\bar{J}_q(\eta - \eta_0)}, & (K = \dfrac{1}{r}\dfrac{\partial r}{\partial s}). \end{cases} \tag{36}$$

Substituting equation (35) into (34), the singular integral $I_{(p,q)}$ can be rewritten by

$$I_{(p,q)} = \bar{J}_p \bar{J}_q \int_{-h_x/2}^{h_x/2} w_p \int_{-h_y/2}^{h_y/2} K_s w_q d\eta \; d\xi + \bar{J}_p \bar{J}_q \int_{-h_x/2}^{h_x/2} w_p \int_{-h_y/2}^{h_y/2} (K - K_s) w_q d\eta \; d\xi. \tag{37}$$

In these integrals, the first term of the right-hand side is calculated analytically, which stems from that we can describe $\eta_0(\xi)$ as a linear transformation $\eta(\xi) = a_1\xi + a_0$ (a_0, a_1: constants). On the other hand, the second term is evaluated using the wavelet-weighted formulae. Since the integrand $(K - K_s)$ is no longer singular kernel, this integral can be calculated by numerical procedure.

Secondary, let us consider a double integral with nearly-singularity. The nearly-singularity occurs in the integrands concerning six kernels: $\ln r$, $\frac{1}{r}\frac{\partial r}{\partial n}$, $\frac{1}{r}\frac{\partial r}{\partial s}$ and $\frac{1}{r}\frac{\partial r}{\partial n}\frac{\partial r}{\partial x_i}\frac{\partial r}{\partial x_j}$ $(i,j = 1,2)$. To ensure a sufficient accuracy for the numerical integration, we employ the subtraction approach analogous to the above regularization scheme as a smoothing technique. We thus deal with the following integrals in order to remove the nearly-singularity of the integrand:

$$I_{(p,q)} = \bar{J}_p \bar{J}_q \int_{-h_x/2}^{h_x/2} w_p \int_{-h_y/2}^{h_y/2} K_v w_q d\eta \; d\xi + \bar{J}_p \bar{J}_q \int_{-h_x/2}^{h_x/2} w_p \int_{-h_y/2}^{h_y/2} (K - K_v) w_q d\eta \; d\xi, \tag{38}$$

where K_v is the nearly-singular term included in the kernel K. In implementation of integration, the nearly-singular term K_v is separated from K by its Taylor expansion around the closest point on supp w_q to a source point. Since K_v is defined as either a logarithmic function or a rational function of η, and the integrals concerning K_v can be calculated analytically with respect to η. By defining $I_v(\xi)$ as

$$I_v(\xi) := \int_{-h_y/2}^{h_y/2} K_v w_q \, d\eta, \tag{39}$$

equation (38) is rewritten by

$$I_{(p,q)} = \bar{J}_p \bar{J}_q \int_{-h_x/2}^{h_x/2} w_p I_v d\xi + \bar{J}_p \bar{J}_q \int_{-h_x/2}^{h_x/2} w_p \int_{-h_y/2}^{h_y/2} (K - K_v) w_q d\eta \, d\xi. \tag{40}$$

In equation (40), the remaining integrals are evaluated by a numerical integration scheme. Like singular integrals, the second term of the right-hand side can be straightforwardly calculated by applying twice the wavelet-weighted formulae, because the integrand $K - K_v$ is sufficiently smooth. Its first term however, has the kernel function $I_v(\xi)$ with wide variation according to circumstances. In this situation, the present strategy is no longer available, and hence we have to utilize other smoothing techniques, e.g. widely-used subelement approach [22] and non-linear transformation [23]. Then, we must use the Gauss-Legendre formula as a numerical integration scheme, instead of the wavelet-weighted formulae.

4.3. Availability of matrix compression scheme

We first verify the validity of the present matrix compression strategy in which the truncation of small entries is applied to the matrix coefficients of boundary element equation (31) with the rearrangement introduced in Section 3.2. As presented in the preceding section, the selection of truncated entries is carried out twice: before and after the assembly of boundary element equations. *A priori* truncation before assembly requires estimation of the matrix coefficients. In this study, we generate *a priori* estimates $\bar{g}^{(\alpha)}_{(w_p,w_q)}$ and $\bar{h}^{(\alpha)}_{(w_p,w_q)}$ in equations (28) and (29) by derivative-type approach as follows:

$$\bar{g}^{(\alpha)}_{(w_p,w_q)} := \begin{cases} \dfrac{c_p c_q \bar{J}_p \bar{J}_q}{8\pi G^{(\alpha)}(1-\nu^{(\alpha)})} \cdot \dfrac{h_x h_y^2 \bar{J}_q}{4} \cdot \dfrac{5-4\nu^{(\alpha)}}{\bar{r}}, & (w_p = \phi,\ w_q = \psi), \\ \dfrac{c_p c_q \bar{J}_p \bar{J}_q}{8\pi G^{(\alpha)}(1-\nu^{(\alpha)})} \cdot \dfrac{h_x^2 h_y \bar{J}_p}{4} \cdot \dfrac{5-4\nu^{(\alpha)}}{\bar{r}}, & (w_p = \psi,\ w_q = \phi), \\ \dfrac{c_p c_q \bar{J}_p \bar{J}_q}{8\pi G^{(\alpha)}(1-\nu^{(\alpha)})} \cdot \dfrac{h_x^2 h_y^2 \bar{J}_p \bar{J}_q}{16} \cdot \dfrac{5-4\nu^{(\alpha)}}{\bar{r}^2}, & (w_p = \psi,\ w_q = \psi), \end{cases} \tag{41}$$

$$\bar{h}^{(\alpha)}_{(w_p,w_q)} := \begin{cases} \dfrac{c_p c_q \bar{J}_p \bar{J}_q}{4\pi(1-\nu^{(\alpha)})} \cdot \dfrac{h_x h_y^2 \bar{J}_q}{2} \cdot \dfrac{5-2\nu^{(\alpha)}}{\bar{r}^2}, & (w_p = \phi,\ w_q = \psi), \\ \dfrac{c_p c_q \bar{J}_p \bar{J}_q}{4\pi(1-\nu^{(\alpha)})} \cdot \dfrac{h_x^2 h_y \bar{J}_p}{2} \cdot \dfrac{5-2\nu^{(\alpha)}}{\bar{r}^2}, & (w_p = \psi,\ w_q = \phi), \\ \dfrac{c_p c_q \bar{J}_p \bar{J}_q}{4\pi(1-\nu^{(\alpha)})} \cdot \dfrac{h_x^2 h_y^2 \bar{J}_p \bar{J}_q}{4} \cdot \dfrac{5-2\nu^{(\alpha)}}{\bar{r}^3}, & (w_p = \psi,\ w_q = \psi), \end{cases} \tag{42}$$

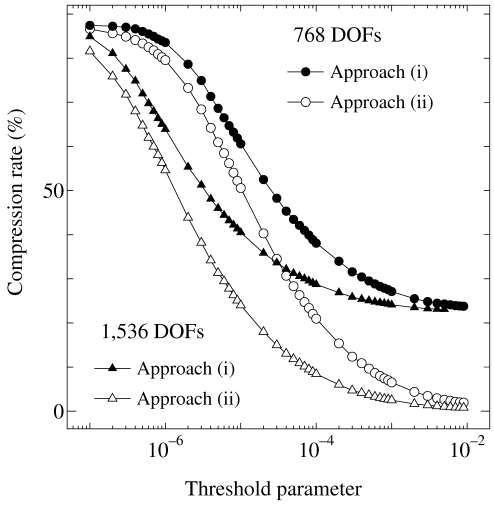

Figure 5: Influence of truncation strategy on compression rates of the coefficient matrix. (Ex.1)

where $\bar{r} := \mathrm{dist}(\mathrm{supp}\ w_p,\ \mathrm{supp}\ w_q)$.

The validity of the present compression strategy is discussed based on the results of numerical tests: we chose Ex.1 as the test example. In numerical experiments, the truncation of small matrix entries was applied to either

(i). the matrix entries $g^{(\alpha)}_{(p,q)(i,j)}$ and $h^{(\alpha)}_{(p,q)(i,j)}$ of original boundary element equations (18) and (19), or

(ii). the matrix coefficients obtained by assembling boundary element equation (31).

Note that in approach (i) the continuous and equilibrium conditions (21) on $\bar{S}$ and $\bar{\Gamma}$ and rearrangements (25) are imposed on equations (18) and (19) after truncation. We show the compression rates of the resulting matrix under the above alternatives in Figure 5. Approach (ii) presented in the preceding section yields higher compression rates of the system matrix than that for approach (i); besides, predominance of approach (ii) on sparseness is independent of the truncation tolerance τ. The same tendency as the present results has been found for other examples, though we omit to indicate these results. As a result, we can conclude that approach (ii) provides higher matrix compression rates than approach (i) under the same threshold.

We next investigate the justification of the optimal threshold parameter determined by the practical strategy developed in Ref. [18]. In this study, the optimal threshold parameter was set to

$$\tau := \min_{kl=11,22,33,12} \frac{\|\mathbf{c}^{kl}\|}{2\|\mathbf{H}^{(2)}\| \cdot \|\boldsymbol{\chi}^{kl}\|} \approx \frac{1}{2\|\bar{\mathbf{H}}^{(2)}\|} \min_{kl} \alpha^{(kl)} \mathscr{N}^{-\beta^{(kl)}}, \tag{43}$$

$$\mathbf{c}^{kl} := \{c^{kl}_{p,i}\},$$
$$c^{kl}_{(p,i)} := -\frac{1}{2}\delta_{ij} \int_{\bar{S}+\bar{\Gamma}} w_p(\chi^{kl}_j - \hat{\chi}^{kl}_j)\, d(\partial Y_2) - \int_{\bar{S}+\bar{\Gamma}} w_p \int_{\bar{S}+\bar{\Gamma}} p^{(2)*}_{ij}(\chi^{kl}_j - \hat{\chi}^{kl}_j)\, d(\partial Y_2), \tag{44}$$

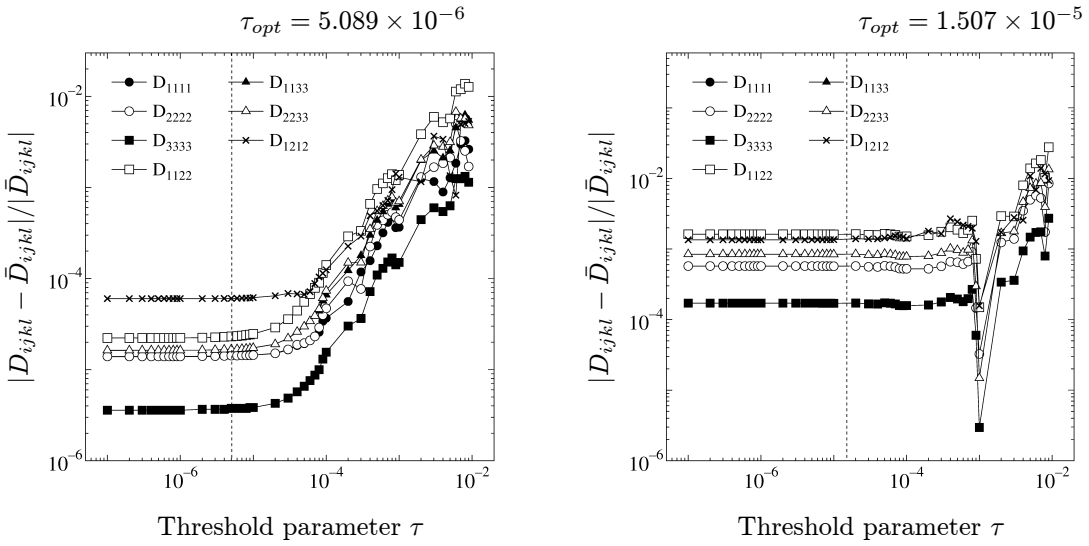

(a) Ex.1. (1,536 DOFs)

(b) Ex.2. (1,024 DOFs)

Figure 6: Influence of the threshold parameter τ on the relative errors of effective elastic moduli. $\bar{D}_{ijkl}$ was evaluated by the BE solution $\tilde{\boldsymbol{\chi}}^{kl}$ with a sufficient large DOF. $\left(\text{Ex.1 and Ex.2, } \tau := \min_{kl} \frac{||\mathbf{c}^{kl}||}{2 \cdot ||\mathbf{H}|| \cdot ||\boldsymbol{\chi}^{kl}||}\right)$

where $\mathscr{N}$ is the degree of freedom of simultaneous equation (31). $\hat{\chi}_j^{kl}$ is the wavelet expansion of the true solution of the characteristic function χ_j^{kl}. Since $(\chi_j^{kl} - \hat{\chi}_j^{kl})$ cannot be exactly evaluated in general, we approximate it as follows:

$$\chi_j^{kl} - \hat{\chi}_j^{kl} \approx \check{\chi}_j^{kl} - \tilde{\chi}_j^{kl}, \tag{45}$$

where $\check{\chi}_j^{kl}$ is a higher-order interpolation of the BE solution $\tilde{\chi}_j^{kl}$.

In the present determination strategy, we originally need to evaluate $\|\mathbf{c}^{kl}\|/\|\boldsymbol{\chi}^{kl}\|$ and $\|\mathbf{H}^{(2)}\|$ corresponding to the approximate solution with the same DOF as the main analysis. Such evaluation is however, unrealistic due to the expensive computational cost of pre-processing for determining the thresholding value. Hence, the value of $\|\mathbf{c}^{kl}\|/\|\boldsymbol{\chi}^{kl}\|$ is estimated using the approximate expression $\alpha^{(kl)}\mathscr{N}^{-\beta^{(kl)}}$: the parameters $\alpha^{(kl)}$ and $\beta^{(kl)}$ are set in advance based on the BE solutions corresponding to sufficient small DOFs. $\|\mathbf{H}^{(2)}\|$ is also approximated by the norm of a small-size matrix $\bar{\mathbf{H}}^{(2)}$ used in the determination process of the parameters $\alpha^{(kl)}$ and $\beta^{(kl)}$.

Now, the thresholding value τ determined by equation (43) is validated based on the relative errors of the effective elastic moduli D_{ijkl}. We show the relation between the threshold parameters and the relative errors of D_{ijkl} in Figure 6. The numerical results indicate the behavior of the relative errors in homogenization analyses for Ex.1 ($\mathscr{N} = 1,536$) and Ex.2 ($\mathscr{N} = 1,024$). Moreover, the dashed line shows the level of the optimal threshold parameter τ evaluated by equation (43). Notice that in this stage τ is calculated using the true value of $\|\mathbf{c}^{kl}\|/\|\boldsymbol{\chi}^{kl}\|$ in order to remove the influence of approximation error.

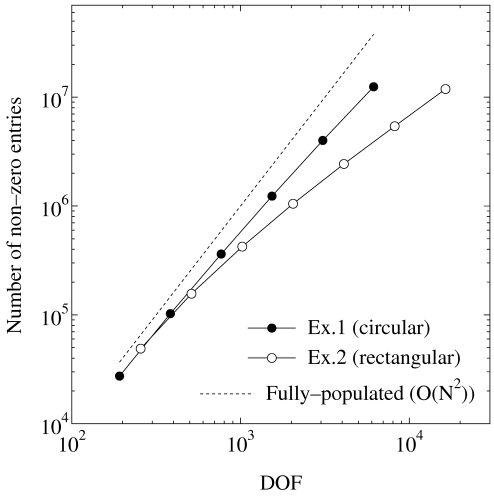

Figure 7: The number of non-zero entries of the coefficient matrix.

Under the optimal value τ, the relative errors of D_{ijkl} are comparable to the errors for sufficiently small thresholding values, which implies that the truncation using the estimated value of τ does not cause overtruncation and deterioration of accuracy of the effective moduli. Since the error due to the truncation under a smaller thresholding value is negligible in comparison with the discretization error, the relative error can be regarded as discretization error. Besides, the relative error increases in the range where the threshold parameter is over the value of τ. A sequence of the above facts indicates that the practical strategy developed in Ref.[18] enables us to accurately determine the optimal value of the threshold parameter in the homogenization analysis.

The number of non-zero entries of the coefficient matrix under each DOF is shown in Figure 7. The number of non-zero entries has a dependency on degrees of freedom of $O(\mathcal{N}^{1+\gamma})$ $(0 \leq \gamma < 1)$ for the present truncation method. In these examples, we obtained $\gamma = 0.76$ (Ex.1) and $\gamma = 0.32$ (Ex.2), i.e., $O(\mathcal{N}^{1.76})$ and $O(\mathcal{N}^{1.32})$ complexity. Unfortunately, the Beylkin-type algorithm proposed in Ref. [18] does not have the complexity of $O(\mathcal{N}(\log \mathcal{N})^{\alpha})$. However, since the matrix compression reduces the order of complexity from $O(\mathcal{N}^2)$ (dotted line) to $O(\mathcal{N}^{1+\gamma})$ (solid lines), application of wavelet BEMs yields the remarkable computational merit — higher compression rate of the coefficient matrix — in the range of larger DOF, especially for Ex.2.

4.4. Effectiveness of rearrangement of boundary element equation on acceleration of iterative process

As presented in Section 3.2, we construct the rearrangement algorithm for boundary element equation (22) as a preconditioner for the coefficient matrix in which dominant elements do not always distribute in the vicinity of matrix diagonal. This subsection is devoted to the verification of effectiveness of the rearrangement introduced in equation (31). In numerical experiments, the system matrix of boundary element equations is

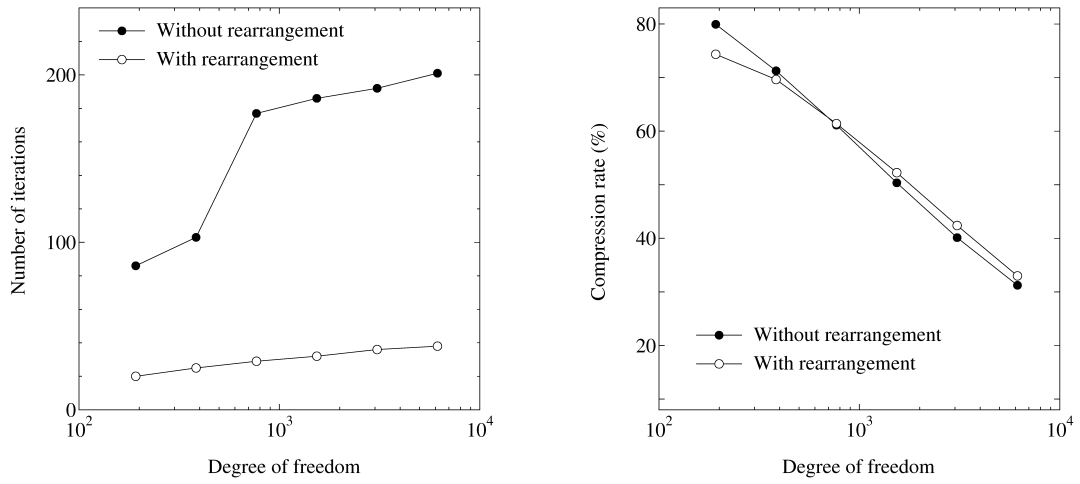

(a) Number of iterations for solving BE equation.

(b) Compression rate of the coefficient matrix.

Figure 8: Influence of rearrangement of BE equation on computational performance in Ex.1.

compressed by approach (ii) presented in the preceding subsection. Hence, the truncation of small matrix entries is carried out to algebraic equation (26) or (31).

We first depict the number of iterations for solving of the boundary element equations in Figure 8(a). Here we show the numerical results for Ex.1. In numerical analysis, we adopted the restart version of the preconditioned GMRES [24] as a solver; the restart parameter was set to 100. Moreover, the Jacobi preconditioning was used in the iterative process, in addition to the present rearrangement process. For the boundary element equations without rearrangement, about 200 iterations are required to attain the convergence when the DOF is greater than $1,000$. This large number of iterations is however, decreased drastically by application of the present rearrangement algorithm: in this example with the rearrangement the number of iterations was $20 - 40$ times. In other words, we were able to achieve $1/4 - 1/5$ saving of computational work for solving the boundary element equations. Note that the present rearrangement is effective for any DOF, as shown in Figure 8(a). Thus, we can conclude that the rearrangement introduced in Section 3.2 is robust for increase in DOFs.

Next, let us consider the influence of rearrangement on the sparseness of the coefficient matrix. We show the compression rate of the system matrix with and without rearrangement, in Figure 8(b). Since the rearrangement introduced in Section 3.2 requires the addition and subtraction of matrix entries, the sparseness of the coefficient matrix seems to be changed by the rearrangement. Indeed, the number of non-zero entries is scarcely influenced by application of the present rearrangement algorithm, as shown in Figure 8(b). This manipulation does not lead to the decay of sparseness.

Through a sequence of numerical results, we have verified the effectiveness of the pro-

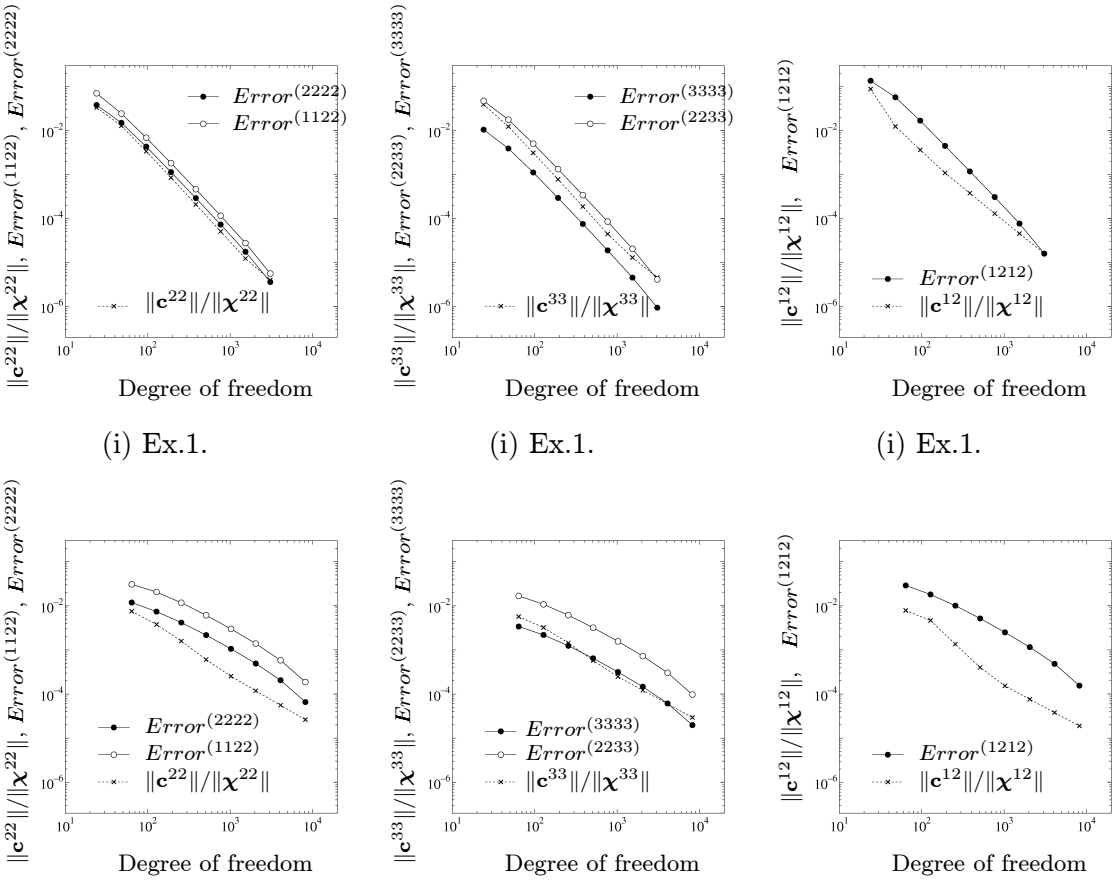

(i) Ex.1. (i) Ex.1. (i) Ex.1.

(ii) Ex.2. (ii) Ex.2. (ii) Ex.2.

(a) D_{1122} and D_{2222}. (b) D_{2233} and D_{3333}. (c) D_{1212}.

Figure 9: Relative errors of effective elastic moduli D_{1122}, D_{2222}, D_{3333}, D_{2233} and D_{1212}, and the residual norm $\|\mathbf{c}^{kl}\|/\|\boldsymbol{\chi}^{kl}\|$. (Ex.1 and Ex.2, $Error^{(ijkl)} := |D_{ijkl} - \bar{D}_{ijkl}|/|\bar{D}_{ijkl}|$ where the value of $\bar{D}_{ijkl}$ was evaluated by the BE solution $\tilde{\boldsymbol{\chi}}^{kl}$ with a sufficient large DOF.)

posed rearrangement algorithm, and have shown that the present matrix compression enables us to reduce the computational cost of BE-based homogenization analysis. However, the above discussion may be no longer consistent for microstructure with some inclusion. This is based on the following two facts: (i) we dealt with the heterogeneous media with microscopic voids in the present examples. And (ii) the rearrangement of equations for the microscopic problems with inclusion yields many fill-in entries. As a result, equation (26) to which the present rearrangement algorithm is applied has quite different non-zero population of the matrix, in comparison with equation (22) without rearrangement. Therefore, we will need to further investigate the sparseness of the system matrix in this situation.

4.5. Asymptotical convergence of effective elastic modulus

As mentioned in Section 1, the homogenization analyses using the BEM have been attempted by several engineers. Their attempts are based on the advantages of the BEM: the easy generation of boundary elements and the accurate evaluation of the effective elastic moduli. Okada et al. [6] have discussed the relation between the evaluated values of the effective moduli and the number of boundary elements; however, the behavior of errors included in the effective moduli have not been clarified. We thus investigate the errors of homogenized elastic moduli, from a viewpoint of asymptotical convergence.

Figure 9 depicts the relation between DOFs and the relative errors of the effective elastic moduli D_{1122}, D_{2222}, D_{3333}, D_{2233} and D_{1212}. We present the numerical results corresponding to Ex.1 and Ex.2 in this figure; besides, the values of the residual norms $\|\mathbf{c}^{kl}\|/\|\boldsymbol{\chi}^{kl}\|$, indicating the discretization error of BE solutions, are also shown in order to compare with the asymptotical convergence rates of $\boldsymbol{\chi}^{kl}$. In this figure, $Error^{(ijkl)}$ stands for the relative error of D_{ijkl} and is defined by

$$Error^{(ijkl)} := \frac{|D_{ijkl} - \bar{D}_{ijkl}|}{|\bar{D}_{ijkl}|},$$

where D_{ijkl} is the effective modulus evaluated by the present scheme. And $\bar{D}_{ijkl}$ is the true value of the effective modulus. In the present example, we use the value evaluated by the BE solution with a sufficient large DOF for $\bar{D}_{ijkl}$.

In the evaluation of effective elastic moduli, we computed the values of D_{ijkl} by boundary integral form (13) which consisted of a boundary integral concerning $\boldsymbol{\chi}^{kl}$. Hence, the effective moduli D_{ijkl} converge roughly with the same asymptotical rates as those of the characteristic functions $\boldsymbol{\chi}$. Note that the rate of convergence in Ex.2 is lower than in Ex.1 because of the existence of singularity. Okada et al. [6] have pointed out that the BEM enables us to accurately evaluate the effective elastic moduli even under small DOFs. The justification of such suggestion may be verified by the present investigation from a viewpoint of asymptotical convergence of both $\boldsymbol{\chi}^{kl}$ and D_{ijkl}.

Next, let us consider the relation between the void size and the errors of the effective elastic moduli. The errors of 5 components D_{1111}, D_{1122}, D_{1133}, D_{3333} and D_{1212} under several void sizes L_1 in Ex.2 are shown in Figure 10. D_{1111}, D_{1133} and D_{3333} scarcely depend on the void size, while the errors of D_{1122} and D_{1212} are sensitive to the size L_1. In particular, the components D_{1212} is very sensitive to large size of rectangular void. The stress concentration at the corners of rectangular voids will cause the reduction of accuracy on the effective moduli. In this situation, we have to set the DOF of the BE solution $\tilde{\boldsymbol{\chi}}^{kl}$ to a larger number, in order to ensure the accuracy of all components of D_{ijkl} for large void size.

As mentioned above, the effective elastic moduli can be efficiently evaluated by the BE-based homogenization approach. If a phase of microstructure is simple one like Ex.1 and Ex.2, we will be able to estimate the effective moduli with very small DOF. However, for the microstructures with many inclusions or voids, e.g. Ex.3, we cannot avoid dealing with a large-scale problem. In this situation, the main drawback of BE analysis —

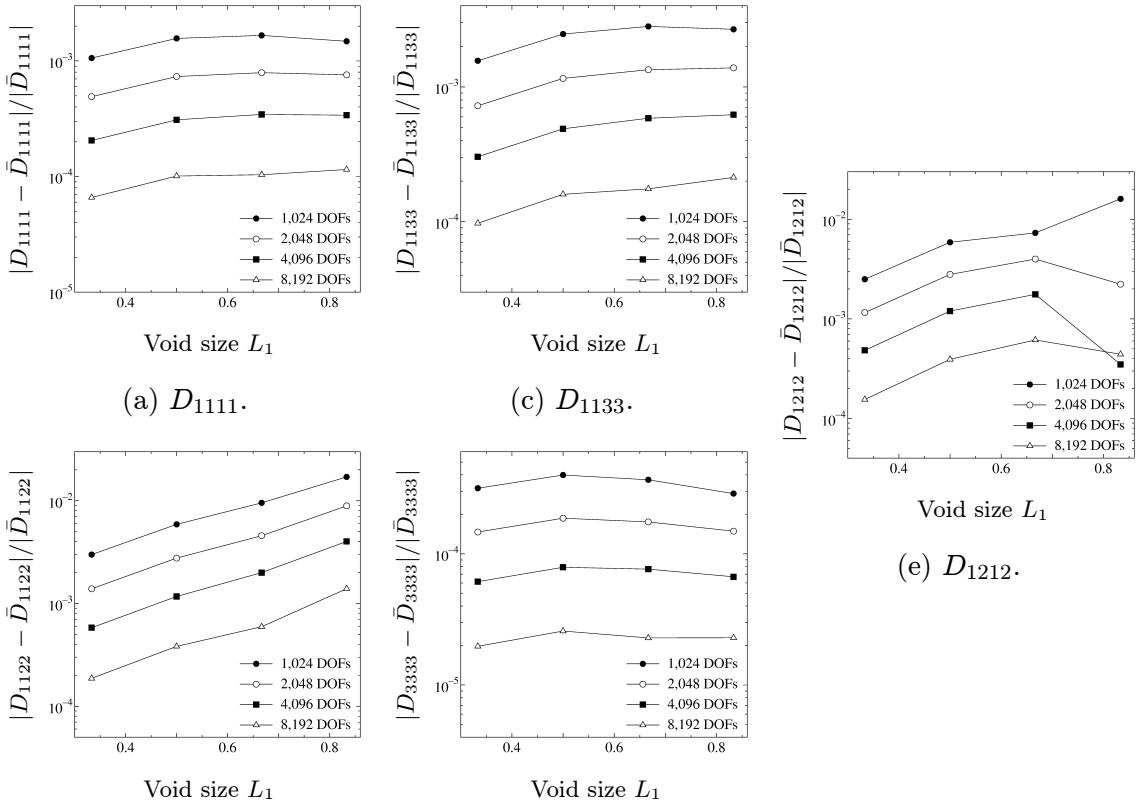

(a) D_{1111}. (c) D_{1133}. (e) D_{1212}.

(b) D_{1122}. (d) D_{3333}.

Figure 10: Relation between the relative errors of effective elastic moduli and the void size L_1 in Ex.2.

large computational cost — becomes an essential obstacle. To overcome this difficulty, application of the wavelet BEM to the homogenization analysis will be effective. We now tabulate the resulting effective moduli, the thresholding values, the compression rates of the system matrix and the overall CPU time for the homogenization analysis, in Table 1. Note that the numerical results presented in this table correspond to Ex.3 and Ex.4 shown in Figure 4. In the present homogenization analyses, 50 – 80 % of memory requirements of conventional BE analyses were saved using the wavelet BEM. Although the case of 5,888 DOF in Ex.3 has almost the same number of stored entries as the case of 5,632 DOF in Ex.4, the former spends three times of CPU time of the latter. The reason is that the numerical integrations are used in Ex.3 and these spend much computation time.

5 Conclusions

In the present paper, we have introduced homogenization analysis using the wavelet BEM, and have attempted to reduce the computational cost for the BE-based homoge-

Table 1: The homogenized elastic moduli evaluated by the wavelet BEM and the computational cost of the homogenization analysis. (Ex.3 and Ex.4. τ is the optimal threshold parameter, which is set by the present determination strategy.)

(a) Ex.3.

	1,492 DOFs	2,944 DOFs	5,888 DOFs
D_{1111}	0.67001	0.66155	0.65897
D_{2222}	0.66913	0.66122	0.65922
D_{3333}	0.92954	0.92716	0.92655
D_{1122}	0.23784	0.23279	0.23166
D_{1133}	0.27235	0.26830	0.26719
D_{2233}	0.27209	0.26820	0.26726
D_{1212}	0.10898	0.10373	0.10214
τ	1.829×10^{-4}	5.031×10^{-5}	1.319×10^{-5}
Comp. rate (%)	46.81	40.74	34.29
CPU time (sec)	336.37	940.36	3213.90

(b) Ex.4.

	2,816 DOFs	5,632 DOFs	11,264 DOFs
D_{1111}	0.47872	0.48252	0.48477
D_{2222}	0.47872	0.48252	0.48477
D_{3333}	0.80907	0.81011	0.81082
D_{1122}	0.11424	0.11623	0.11793
D_{1133}	0.17789	0.17962	0.18081
D_{2233}	0.17789	0.17962	0.18081
D_{1212}	0.08954	0.09155	0.09254
τ	1.914×10^{-5}	9.173×10^{-6}	4.458×10^{-6}
Comp. rate (%)	54.19	35.60	21.66
CPU time (sec)	379.39	906.11	2349.81

nization analysis. The formulation for microscopic problems using the wavelet BEM has been described. Besides, we have introduced additional numerical techniques: the matrix compression, the determination of an optimal threshold parameter and the rearrangement of boundary element equations.

The compression scheme and the determination strategy of the optimal thresholding value have been constructed based on the scheme developed in Ref. [18]. The matrix compression using their algorithms is available for the present 2-D elastostatic homogenization analysis. Since the threshold parameter can be adequately set by the heuristic approach, the implementation of wavelet BEM is effective in the homogenization analysis.

On the other hand, the algorithm of the equation rearrangement has been constructed as a preconditioner to solve the boundary element equations using an iterative solver. In the BE-based homogenization analysis, we assemble a system of algebraic equations through imposing periodicity conditions of microstructures. Then, the resulting equations have the coefficient matrix where dominant entries are not always populated in the vicinity of diagonal. When we solve these equations with an iterative solver, such a matrix population causes the increase in the number of iterations, in general. This computational problem can be settled by application of the rearrangement scheme. In the present numerical experiments, we have achieved the reduction of the computational work for iterations up to $1/4 - 1/5$ of that for the simultaneous equations without rearrangement.

Finally, we have investigated the behavior of errors in the effective elastic moduli evaluated by BE-based homogenization analysis. Since the effective moduli are evaluated by boundary integrals with the microscopic perturbed displacements $\boldsymbol{\chi}^{kl}$, we have obtained the same asymptotical convergence rates as those of BE solutions $\tilde{\boldsymbol{\chi}}^{kl}$. As mentioned in Ref. [6] and this paper, the BE-based approach enables us to accurately evaluate the effective moduli even under small DOF. However, we will certainly encounter rising of computational cost, if we apply the homogenization method to heterogeneous media with complicated phases of microstructures. In addition, a large system of BE equations has to be dealt with for microscopic problems with large size voids or with stress concentrations. Then, application of the wavelet BEM will be effective for the reduction of computational cost in BE analysis. In the present study we employed the wavelet BEM as a numerical tool in the microscopic analysis for heterogeneous media with many voids: the effective elastic moduli with agreement of $2 - 4$ digits can be evaluated using $20 - 50$ % memory requirements of conventional BE approaches.

References

[1] Hashin Z. Analysis of composite materials – a survey. Journal of Applied Mechanics ASME 1983; 50: 480–505.

[2] Hollister SJ, Kikuchi N. A comparison of homogenization and standard mechanics analyses for periodic porous composites. Computational Mechanics 1992; 10: 73–95.

[3] Guedes JM, Kikuchi N. Preprocessing and postprocessing for materials based on the homogenization method with adaptive finite element methods. Computer Methods in Applied Mechanics and Engineering 1990; 83: 143–198.

[4] Michel JC, Moulinec H, Suquet P. Effective properties of composite materials with periodic microstructure: a computational approach. Computer Methods in Applied Mechanics and Engineering 1999; 172: 109–143.

[5] Terada K, Kikuchi N. A class of general algorithms for multi-scale analyses of heterogeneous media. Computer Methods in Applied Mechanics and Engineering 2001; 190: 5427–5464.

[6] Okada H, Fukui Y, Kumazawa N. Homogenization method for heterogenious material based on boundary element method. Computers & Structures 2001; 79: 1987–2007.

[7] Kamiński M. Boundary element method homogenization of the periodic linear elastic fiber composites. Engineering Analysis with Boundary Elements 1999; 23: 815–823.

[8] Procházka P. Shape optimization of composites using the BEM. Boundary Element Technology XIII, Chen CS, Brebbia CA, Pepper DW, eds., WIT Press, Southampton, Boston, 1999: 89–98.

[9] Procházka P. Homogenization of linear and of debonding composites using the BEM. Engineering Analysis with Boundary Elements 2001; 25: 753–769.

[10] Dahmen W, Prösdorf S, Schneider R. Wavelet approximation methods for pseudodifferential equations II: Matrix compression and fast solution. Advances in Computational Mathematics 1993; 1: 259–335.

[11] Beylkin G, Coifman R, Rokhlin V. Fast wavelet transforms and numerical algorithms I. Communication on Pure and Applied Mathematics 1991; 44: 141–183.

[12] Goswami JC, Chan AK, Chui CK. On solving first-kind integral equations using wavelets on a bounded interval. IEEE Transactions on Antennas and Propagation 1995; 43(6): 614–622.

[13] von Petersdorff T, Schwab C. Wavelet approximations for first kind boundary integral equations on polygons. Numerische Mathematik 1996; 74: 479–519.

[14] Wang G. Application of wavelets on the interval to numerical analysis of integral equations in electromagnetic scattering problems. International Journal for Numerical Methods in Engineering 1997; 40: 1–13.

[15] Rathsfeld A. A wavelet algorithm for the boundary element solution of a geodetic boundary value problem. Computer Methods in Applied Mechanics and Engineering 1998; 157: 267–287.

[16] Lage C, Schwab C. Wavelet Galerkin algorithms for boundary integral equations. SIAM Journal on Scientific Computing 1999; 20(6): 2195–2222.

[17] Koro K, Abe K. Non-orthogonal spline wavelets for boundary element analysis. Engineering Analysis with Boundary Elements 2001; 25: 149–164.

[18] Koro K, Abe K. Determination of optimal threshold for matrix compression in wavelet BEM. Boundary Elements XXIII, Bescos DE, Brebbia CA, Katsikadelis JT, Manolis GD, eds., WIT Press, Southampton UK, 2001: 475–484.

[19] Abe K, Koro K. Gauss quadrature method using wavelet basis as a weighting function for boundary element analysis. Boundary Elements XXIII, Bescos DE, Brebbia CA, Katsikadelis JT, Manolis GD, eds., WIT Press, Southampton UK, 2001: 455–464.

[20] Parreira P, Guiggiani M. On the implementation of the Galerkin approach in the boundary element method. Computers & Structures 1989; 33(1): 269–279.

[21] Guiggiani M, Gigante A. A general algorithm for multi-dimensional Cauchy principal value integrals in the boundary element method. Journal of Applied Mechanics ASME 1990; 57: 906–915.

[22] Lachat JC, Watson JO. Effective numerical treatment of boundary integral equations: a formulation for three-dimensional elastostatics. International Journal for Numerical Methods in Engineering 1976; 10: 991-1005.

[23] Telles JCF. A self-adaptive co-ordinate transformation for efficient numerical evaluation of general boundary element integrals. International Journal for Numerical Methods in Engineering 1987; 24: 959–973.

[24] Saad Y, Schultz MH. GMRES: A generalized minimal residual algorithm for solving nonsymmetric linear system. SIAM Journal on Scientific Statistical Computing 1986; 7(3): 856–869.